Voltage gated ion and molecule transport in engineered nanochannels: theory, fabrication and applications

2014 Nanotechnology 25 122001

(http://iopscience.iop.org/0957-4484/25/12/122001)

IOP Publishing Nanotechnology
Nanotechnology **25** (2014) 122001 (19pp) doi:10.1088/0957-4484/25/12/122001

Topical Review

Voltage gated ion and molecule transport in engineered nanochannels: theory, fabrication and applications

Weihua Guan[1], **Sylvia Xin Li**[2] **and Mark A Reed**[1,3]

[1] Department of Electrical Engineering, Yale University, New Haven, CT 06520, USA
[2] Department of Physics, Yale University, New Haven, CT 06520, USA
[3] Department of Applied Physics, Yale University, New Haven, CT 06520, USA

E-mail: weihua.guan@yale.edu and mark.reed@yale.edu

Received 15 September 2013, revised 29 October 2013
Published 25 February 2014

Abstract
Nanochannels remain at the focus of growing scientific and technological interest. The nanometer scale of the structure allows the discovery of a new range of phenomena that has not been possible in traditional microchannels, among which a direct field effect control over the charges in nanochannels is very attractive for various applications, since it offers a unique opportunity to integrate wet ionics with dry electronics seamlessly. This review will focus on the voltage gated ionic and molecular transport in engineered gated nanochannels. We will present an overview of the transport theory. Fabrication techniques regarding the gated nanostructures will also be discussed. In addition, various applications using the voltage gated nanochannels are outlined, which involves biological and chemical analysis, and energy conversion.

Keywords: nanofluidics, voltage gated nanochannels, electrofluidics

(Some figures may appear in colour only in the online journal)

Contents

1. Introduction

With applications ranging from biosensing to the control of ionic and molecular transport, nanochannels are at the focus of growing scientific and technological interest [1]. The nanochannels here refer to a broad range of nanostructures with at least one dimension ranging from 1 to 100 nm, including nanoslits (2D), nanotubes (1D) and nanopores (0D). The nanometer scale of the structure allows the discovery of a new range of phenomena that has not been possible in traditional

microchannels. Over the past few years, much attention has been paid to utilizing the engineered nanochannels as tools for fast and high-throughput biosensors [2], for regulating [3] and separating [4] ions and molecules in electrolyte solutions, and for energy harvesting [5, 6].

Besides the size related steric effects, one of the most important features in a liquid phase nanochannel is the length scale between the Debye length and the channel size. When an electrolyte solution is confined within a channel of a charged surface, counter-ions will accumulate near the charged surface while co-ions are repelled. Due to this effect, the electric potential at the surface will decay to a bulk value over a characteristic length known as the Debye length. The Debye length λ_D decreases as the ion concentration, n, increases $\lambda_D \sim n^{-1/2}$. Typical values for λ_D is 1–100 nm for aqueous solutions. In conventional micrometer-sized channels, the Debye length is usually much smaller than the channel dimensions, and thus the bulk of the solution is shielded from the surface charge. As a result, although interfacial effects such as electro-osmotic flow can be controlled by modulating the surface charge in microchannels [7], direct modulation of ions and molecules by orthogonal gating electric fields is impossible in microchannels. However, nanochannels, which have one dimension comparable to or even smaller than the Debye length, possess an electrostatic potential that can be significantly modulated by external gating voltages. Thus, direct voltage gated ionic and molecular transport in nanochannels becomes feasible.

The transport phenomena in nanoscale channels have been comprehensively reviewed [8–11]. This review is specifically dedicated to voltage gated ionic and molecular transport in engineered gated nanochannels. It is worth noting that the term '*voltage gated*' in this review should not be confused with '*voltage gated ion channels*' in cells [12, 13]. Whereas the '*voltage gated ion channels*' are two-terminal molecular devices that facilitate ion transport across cell membranes, the '*voltage gated nanochannel*' in this review refers to a three(or more)-terminal device that resembles a metal–oxide–semiconductor field effect transistor (MOSFET).

Active modulation of ions and molecules via field effect gating in nanofluidic channels is an attractive technology for various applications, since it offers a unique opportunity to integrate wet ionics with dry electronics seamlessly. This review consists of three parts: (1) transport theory in nanoscale channels, (2) fabrication techniques, which discusses various technological choices to generate gated nanochannel structures via top-down or bottom-up methods, and (3) applications, which will highlight how devices made from the gated nanochannels can be used in fundamental nanoscale sciences and technological applications such as biological and chemical analysis, and energy conversion. Finally, in the conclusion, we discuss challenges and opportunities in voltage gated ion and molecule transport in engineered nanochannels.

2. Theoretical aspects

2.1. Electrostatics in solutions

When a solid surface is in contact with a polarizable electrolyte solution, surface charges will appear at the solid surface [14]. The electrostatic force will therefore naturally attract oppositely charged ions (counter-ions) and repel like charges (co-ions) in the electrolyte to maintain the electro-neutrality. An electrical double layer (EDL) is therefore formed at equilibrium. The Poisson–Boltzmann equation to describe the electrostatic potential profile ψ due to the distribution of different ionic species is given by

$$\nabla^2\psi = -\frac{e}{\varepsilon_0\varepsilon_r}\sum_i n_0 z_i \exp(-z_i e\psi/k_B T), \tag{1}$$

where e is the elementary charge, ε_0 is the permittivity of free space, ε_r is the dielectric constant of the liquid ($\varepsilon_r = 78.5$ for water at 25 °C), n_0 (m^{-3}) is the bulk number density, $n_0 = 10^{-3} N_A c_i$, and z_i is the valence of charge i.

2.1.1. Debye–Hückel approximation. Generally, there is no analytical solution to the Poisson–Boltzmann equation (1). However, the Debye–Hückel theory [15] was developed to give an approximate analytical solution if the potential in the diffuse layer is very small ($z_i e\psi/k_B T \ll 1$). Using the first two terms in the series expansion for the exponential term: $e^{-a} = 1 - a$ for small a, equation (1) becomes

$$\nabla^2\psi = \kappa^2\psi \tag{2}$$

with

$$\kappa^2 = \frac{e^2\sum_i n_0 z_i^2}{\varepsilon_0\varepsilon_r k_B T}. \tag{3}$$

Using the boundary conditions $\lim_{y\to\infty}\psi = 0$, $\lim_{y\to\infty}\nabla\psi = 0$, and $\psi(y=0) = \psi_s$ (here ψ_s is at the beginning of the diffuse layer), the solution of the Debye–Hückel approximation is given by

$$\psi(y) = \psi_s \exp(-\kappa y). \tag{4}$$

Equation (4) states that the potential *in the diffuse layer* decays exponentially with a characteristic distance, known as the Debye length,

$$\lambda_D = \kappa^{-1}. \tag{5}$$

The Debye length is a very important characteristic length scale, which quantitatively describes the thickness of the diffuse layer. It is clear from equations (3) and (5) that the Debye length is a function of the ionic strength.

2.1.2. Gouy–Chapman approximation. The Debye–Hückel model assumes that the potential in the diffuse layer is very small ($z_i e\psi/k_B T \ll 1$), which will not be valid for high surface potentials (highly charged surface). Under such conditions, the Poisson–Boltzmann equation (1) has to be solved numerically. However, for *planar surfaces*, which is the thin double layer limit for a spherical particle, Gouy [16] and Chapman [17] solved the Poisson–Boltzmann equation (1) analytically. Under the assumption of a symmetrical electrolyte where the valence of the co-ion is equal to the valence of the

counter-ion ($|z^+| = |z^-| = z$), the Gouy–Chapman equation is obtained as [14]

$$\tanh\left(\frac{ze\psi(y)}{4k_BT}\right) = \tanh\left(\frac{ze\psi_s}{4k_BT}\right)\exp(-\kappa y). \quad (6)$$

The equation above is valid for any value of the surface potential ψ_s. For small values of $ze\psi_s/4k_BT$, $\tanh(ze\psi_s/4k_BT) \sim ze\psi_s/4k_BT$, and equation (6) reduces to (4). The Debye–Hückel model also shows an exponential decay of the potential to the bulk value through a characteristic length λ_D.

2.1.3. Surface charge determination. The relation between surface charge $Q_{surface}$ and surface potential ψ_s in the Gouy–Chapman model can be expressed by the Grahame equation. It is derived by assuming an electro-neutrality condition. Using the one-dimensional Poisson equation for a symmetrical electrolyte ($|z^+| = |z^-| = z$), and the boundary conditions of $\lim_{y\to\infty} \nabla\psi = 0$, the Grahame equation is obtained as [18]

$$Q_{surface} = \sqrt{8\varepsilon_0\varepsilon_r n_0 k_B T}\sinh\left(\frac{ze\psi_s}{2k_BT}\right) \quad (7)$$

where n_0 is the bulk number density (m^{-3}), $Q_{surface}$ is in units of C m^{-2} and ψ_s is in volts. As a result, measurements of the ζ potential can be used as an indirect way to quantify the surface charges. In addition, electrostatic force microscopy (EFM) [15, 16] and field effects [19] can also be used to quantitatively determine the surface charges.

2.1.4. Ionic conduction.

2.1.4.1. Bulk conductance. The current density $\boldsymbol{J}_i$ carried by an ion i with valence z_i under the electric field $\boldsymbol{E}$, is given by

$$\boldsymbol{J}_i = \sigma_i \boldsymbol{E} \quad (8)$$

with

$$\sigma_i = z_i n_i e\mu_i = 10^{-3} z_i e\mu_i N_A c_i \quad (9)$$

where σ_i is the electrical conductivity of ion i, N_A is Avogadro's constant, n_i is the number density (m^{-3}), c_i is the molar concentration (mol l^{-1}), μ_i is the ion mobility (m^2 (V s)$^{-1}$), which can be related to the diffusion constant D_i by

$$\mu_i = \frac{eD_i}{k_BT}. \quad (10)$$

The conductivity of the whole electrolyte solution, without considering the complex interactions between ions [14], is given by the sum of the contributions of each ion,

$$\sigma = \sum_i \sigma_i = 10^{-3} eN_A \sum_i z_i\mu_i c_i. \quad (11)$$

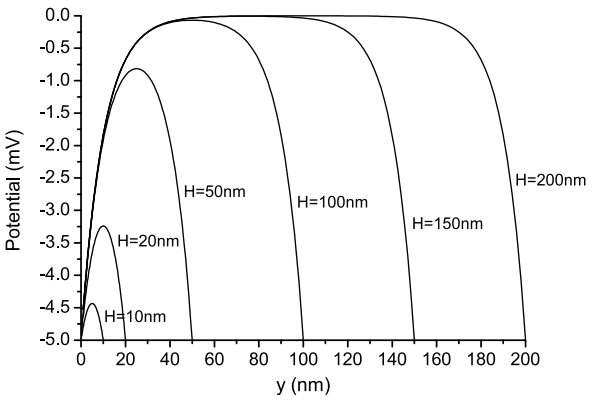

Figure 1. The potential profile $\psi(y)$ for different channel sizes H. The calculation is based on $\zeta = -5$ mV and $\lambda_D = 10$ nm.

2.1.4.2. Surface conductance. The EDL formed around charged surfaces results in an ionic environment that is different from the bulk. This conducting sheet surrounding the charged surface contributes to an additional conductance. The surface conductance can be thought of as a two-dimensional analogue of bulk conduction, with the charge movement confined near the surface.

The surface conductance can be further divided into two separate components, coming from the Stern layer and the diffuse layer, respectively. The total surface conduction G_S can be expressed as the sum of these two components [20],

$$G_S = G_S^{Stern} + G_S^{Diffuse}. \quad (12)$$

For the diffuse layer, the electro-osmotic transport of charge carriers must be considered, in addition to the drift current. The total surface current in the *diffuse* layer is therefore the sum of the drift current J_{Drift} and the electro-osmosis current J_{EO},

$$J_{Diffuse} = J_{Drift} + J_{EO}. \quad (13)$$

2.2. Phenomena in nanoscale channels

2.2.1. Potential profiles in nanochannels. The potential distribution in the case of EDL overlapping in nanochannels with height H, under the Debye–Hückel approximation (low surface potential approximation, see section 2.1.1), is given by [21]

$$\psi(y) = \frac{\zeta\cosh((H/2 - y)/\lambda_D)}{\cosh(H/2\lambda_D)}. \quad (14)$$

Figure 1 shows the electric potential profile for various channel dimensions.

2.2.2. Conductance in nanochannels. The conductance of a nanochannel is the superposition of the bulk conductance and the double layer conductance. For the simple case of a nanochannel filled with KCl solutions, the nanochannel conductance is given by [22, 23]

$$G = e(\mu_K + \mu_{Cl})C_b N_A W H/L + 2\mu_K\sigma_S W/L \quad (15)$$

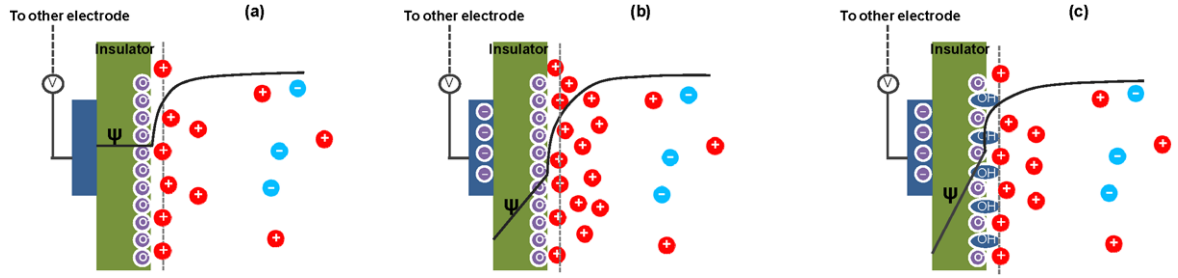

Figure 2. Buffering effect at a chemically reactive surface when applying a perpendicular electric field. (a) At zero bias, a negative surface charge is assumed due to the presence of O^- groups, and an equal but opposite charge resides in the solution. (b) For a chemically inert surface, a negative bias induces extra counter-ions in the diffuse layer. (c) For a chemically reactive surface, additionally attracted protons are buffered by association with the O^- surface groups to form OH groups, decreasing the surface charge density. The counter-ion population in the diffuse layer is less affected. (Reprinted with permission from [36]. Copyright 2009 Royal Society of Chemistry.)

where W (m), L (m) and H (m) are the width, length and height of the nanochannels, respectively. μ_K (m^2 $(V\ s)^{-1}$) and μ_{Cl} (m^2 $(V\ s)^{-1}$) are the mobility of K^+ and Cl^- ions. C_b (mol m^{-3}) is the bulk concentration. N_A (mol^{-1}) is the Avogadro constant, e (C) is the elementary charge and σ_s (C m^{-2}) is the surface charge on the nanochannel walls. For top-down engineered nanochannels, by knowing the dimensions of the lithographically defined channels (W, L), it is possible to derive the value of H in the high-concentration regime (bulk conductance part) and the value of the surface charge σ_s in the low-concentration regime (double layer conductance part) by fitting the experimental data [24, 22, 25].

2.2.3. Permselectivity in nanochannels. Once we know the potential profile in the nanochannel with a characteristic dimension H, the local concentration for ion species i inside the nanochannel can be determined by the Boltzmann equation as

$$n_i(y) = n_0 \exp\left(\frac{-z_i e\zeta \cosh((H/2-y)/\lambda_D)}{k_B T \cosh(H/2\lambda_D)}\right) \quad (16)$$

where n_0 is the bulk number density.

It can be easily calculated from equation (16) that an excess of counter-ions will present inside nanochannels at low ionic strength. This enrichment of counter-ions and exclusion of co-ions in a nanometer-sized channel due to electrostatic interactions with the surface charge is called the exclusion–enrichment effect [26]. When the exclusion and enrichment of ions occurs in nanochannels with low ionic strength, the local concentration of charged species is not homogeneous in the cross section of the nanochannel (equation (16)). The exclusion–enrichment coefficient β_i for ion species i, which is defined as the ratio of the averaged ion concentration to the bulk concentration, can thus be defined as [11]

$$\beta_i = \frac{1}{h}\int_0^h \exp\left(\frac{-z_i e\zeta \cosh((H/2-y)/\lambda_D)}{k_B T \cosh(H/2\lambda_D)}\right) dy. \quad (17)$$

Equation (17) shows the quantitative exclusion–enrichment coefficient depends on the Debye length λ_D, the characteristic dimension of the nanochannel H, the ζ potential at the surface and the charge valence of the ion i. It is easy to see that $\beta_i > 1$ for $z_i\zeta < 0$, which means the counter-ion concentration gets enriched (as compared to the bulk concentration) and $\beta_i < 1$ for $z_i\zeta > 0$, which means the co-ion concentration gets excluded (as compared to the bulk concentration). This results in the permselectivity of the nanochannel.

2.2.4. Field effect control of permselectivity. One of the most important parameters in quantifying the exclusion–enrichment coefficient is the ζ potential at the surface. The ζ potential can be altered by chemical modifications [27, 28]. A more elegant way to change the ζ potential is through an active control with the field effect [3, 29]. In the same way the electric field is used in MOSFETs to regulate the electron/hole population in the silicon conductive channel, the cation and anion population in the nanochannels can be manipulated in a similar fashion. This principle has been used to realize ionic field effect transistors [30–32, 3, 29, 33, 34].

It is worth mentioning that the active control of the permselectivity by using a gating voltage is more than just a physical process, surface chemistry also plays a critical role (figure 2). It has been shown that the chemically reactive surface will behave as a buffer, regulating the charge in the diffuse layer by either protonating or deprotonating in response to the applied field [35]. This buffering effect of a chemically reactive surface is a distinguishing feature of the fluidic version of the field effect [35, 36]. In addition, a recent study also shows that the *bounded* Stern layer will also affect the field effect modulation [37].

2.2.5. Donnan potential. The phenomena above discuss the ions inside the nanochannel and far away from the nanochannel's open end. In reality, an interface between the nanochannel and the adjacent electrolyte solution is inevitable. These two parts will reach *steady-state* when the Gibbs free energy in both parts is identical. This electrochemical equilibrium is referred to as the Donnan equilibrium [38, 39], which is obtained when a concentration difference of the ions between the two parts is compensated by an electrical potential difference. The Donnan potential is analogous to the built-in potential in semiconductor diodes [40].

The electrochemical potential Φ_i of ion i at constant pressure and temperature for an ideal solution (activity coefficient is unity) can be expressed as

$$\Phi_i = \phi_i^0 + RT\ln(c_i/c_0) + z_i F\psi, \tag{18}$$

where ϕ_i^0 is the standard chemical potential of ion i, R is the gas constant, T is the temperature, c_i is the *molar concentration* of ion i (mol l^{-1}, or molar), and c_0 is the standard molarity of 1 molar. F is the Faraday constant, ψ is the electric potential and z_i is the ion valence.

When the nanochannel (N) is in equilibrium with its adjacent bulk electrolyte solution (B), the electrochemical potential for both parts should be equal,

$$\phi_i^0 + RT\ln(c_i^{\mathrm{B}}/c_0) + z_i F\psi^{\mathrm{B}} = \phi_i^0 + RT\ln(c_i^{\mathrm{N}}/c_0) + z_i F\psi^{\mathrm{N}}. \tag{19}$$

As a result, the electric potential difference between the bulk electrolyte solution and the nanochannel region, known as the Donnan potential, can be calculated as

$$\psi^{\mathrm{NB}} = \psi^{\mathrm{N}} - \psi^{\mathrm{B}} = \frac{RT}{z_i F}\ln\left(\frac{c_i^{\mathrm{B}}}{c_i^{\mathrm{N}}}\right). \tag{20}$$

Because of this Donnan potential difference at the micro-nano junction region, ion enrichment and depletion phenomena (or ion concentration polarization) have been observed when applying an electric field across this junction. A detailed discussion of ion concentration polarization phenomena is beyond the scope of this review. Readers are referred to recent review articles by Santiago *et al* [41], Han *et al* [42], and Plecis *et al* [43] for this topic.

3. Fabrication of voltage gated nanochannel

In this section, we will review the fabrication techniques to generate the voltage gated nanochannel structures. Forming a voltage gated nanochannel is related to, yet more complex than the formation of the nanochannel itself. Readers are referred to review articles by Mijatovic *et al* [44] and Perry *et al* [45] regarding two-terminal nanochannel structures. This section will mainly focus on techniques to form nanochannels with gating structures.

3.1. Bottom-up methods

3.1.1. Intrinsic nanochannels. Single-walled carbon nanotubes (SWCNTs) are excellent candidates for nanochannel applications because they have attractive chemical, electronic and mechanical properties [46]. DNA [47] and ion [48, 49] transport through SWCNTs has shown intriguing properties. Gated SWCNT structures can be generated by a hybrid process. Pang *et al* used the bottom-up grown SWCNTs and then subsequently deposited dielectric SiO_2 and gate electrodes on top of the SWCNTs to form the gated nanochannel structure [50].

Another kind of intrinsic nanochannel material consists of various mesoporous membranes, such as mesoporous alumina layers [51] and mesoporous silica [29, 52]. Although the intrinsic properties of individual nanochannels cannot be studied in this kind of system, useful functions can be readily achieved. Fan *et al* reported a dip-coating process for the alignment of uniform SBA-15 mesochannels (pore size < 8 nm) in thin-film (100–200 nm thick) form [29]. They then fabricated gated nanochannel structures based on SBA-15 mesochannels to control the proton transport. As shown in figure 3, the SBA films on quartz or silicon dioxide substrates were patterned by reactive ion etching (RIE) in the CHF_3/CF_4 plasma. Afterwards, Cr/Au electrodes were sputter-deposited and patterned by wet etching. At the same time, a PDMS microfluidic stamp was separately fabricated by soft lithography. Finally, the PDMS chip was bonded onto the mesoporous thin-film sample to form the gated nanochannel structures. The basic fabrication process is very similar to the case of SWCNTs, except that a dielectric layer is not required in the case of SBA films since the channel wall itself is an intrinsic dielectric material.

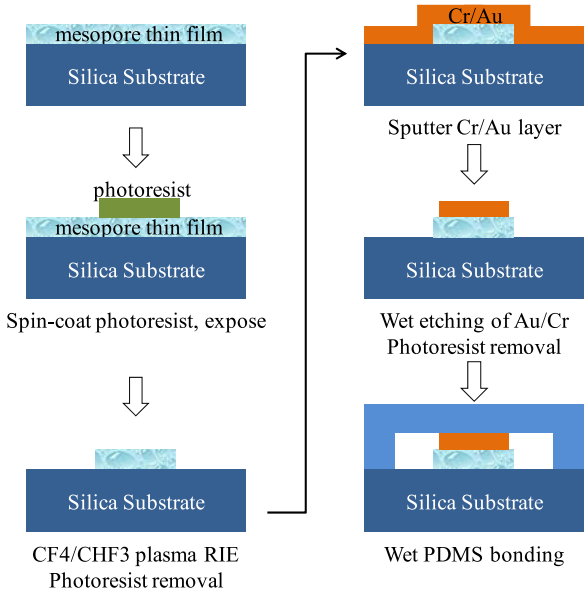

Figure 3. Fabrication process of the gated nanofluidic device based on aligned SBA-15 thin films [29].

It is noteworthy that ion-selective membranes with high surface charges, such as Nafion [53, 54], are not quite suitable for the gated nanochannel structure. This is because an inherent high surface charge density in nanochannels resembles degenerate doping in a semiconductor or high surface state density of a FET, which makes the electrostatic control of the ionic concentration in nanochannels very difficult [3].

3.1.2. Templated nanochannels. Nanochannels can also be formed by template approaches. For example, an epitaxial casting approach to synthesize single crystalline GaN nanotube arrays from ZnO nanowire templates has been demonstrated [55]. In addition, a partial thermal oxidation of bottom-up grown silicon nanowires can lead to hollow silica nanotubes after selective etching of the core (figure 4). The dimension

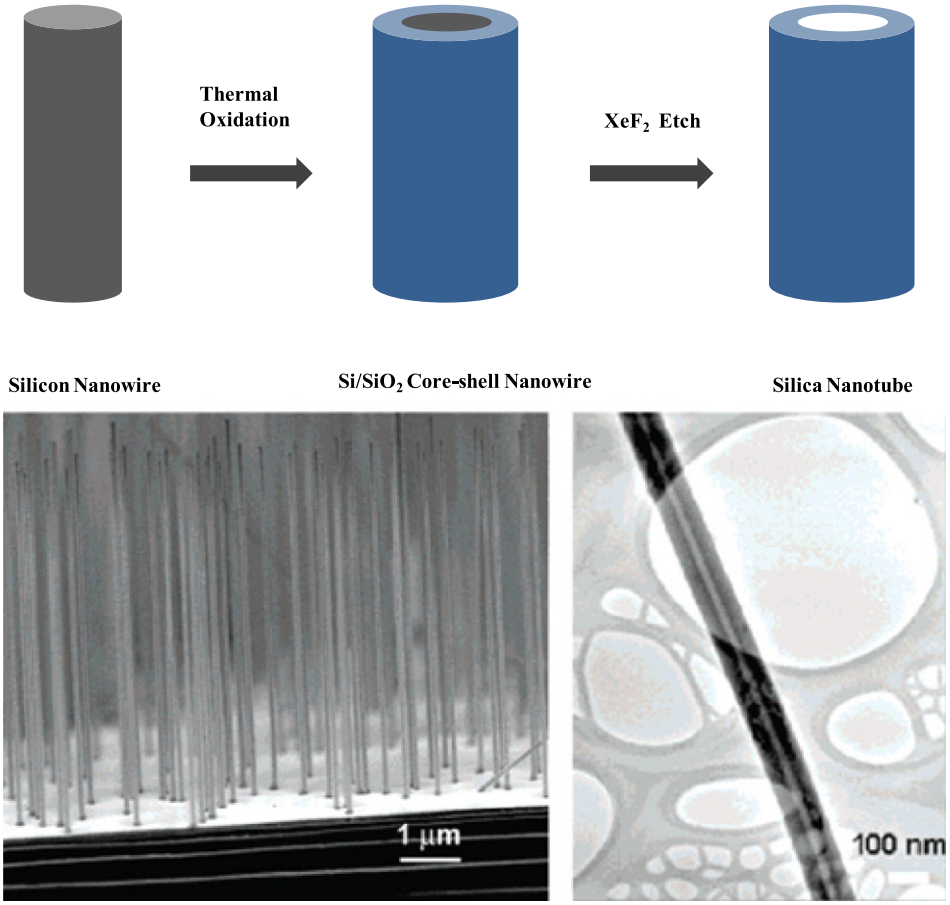

Figure 4. Oxidation–etching approach to synthesize vertical silica nanotube arrays from silicon nanowire templates. The bottom panels show the scanning electron micrographs of the as-grown silicon nanowire array and the transmission electron image of a representative silica nanotube. (Reprinted with permission from [55]. Copyright 2006 American Chemical Society.)

of silica nanotubes can be precisely controlled during the templating process. Those templated nanochannels can then be harvested and made into gated nanochannel structures in a similar way to the SWCNTs [32]. As shown in figure 5, the harvested silica nanotubes can be integrated into a gated nanochannel structure by interfacing with two microfluidic channels made from PDMS. Figure 5(a) shows the schematic of the device and figure 5(b) shows a fully assembled device with a PDMS cover with access holes, which includes source (S)/drain (D) microfluidic channels and the metallic gate electrodes (G).

3.2. Top-down methods

3.2.1. Gated 1D and 2D nanochannels. The drawbacks of the bottom-up techniques using either intrinsic or templated nanochannels are the critical alignment requirement and the low fabrication yield. Gajar and Geis demonstrated the first CMOS compatible process for a gate-all-around nanochannel structure [30]. In their process (figure 6), Si wafers are firstly coated with 2 μm of thermal SiO_2 for electrical insulation. A layer of polysilicon is then chemically vapor deposited (CVD), phosphorus doped, and patterned to form the lower gate electrode. The electrode is electrically and ionically insulated by thin layers of thermal SiO_2 and CVD Si_3N_4, respectively. This forms the lower half of the gated nanochannel. A layer of sacrificial amorphous CVD Si is then deposited and patterned into strips. These strips are covered with thin layers of CVD Si_3N_4 and CVD SiO_2 to form the upper half of the gated nanochannel. A layer of CVD polysilicon is deposited, phosphorus doped, and patterned to form the upper gate electrode, and the whole structure is then covered with 1 μm thick CVD SiO_2. Access to the sacrificial amorphous Si is made by etching the SiO_2 and Si_3N_4 in the source and drain reservoir areas. The amorphous Si is then selectively etched away by tetramethylammonium hydroxide (TMAH). Finally, metal contacts are deposited and patterned with a liftoff process in the gate and reservoir areas.

Variations of this sacrificial layer method have been widely adopted by researchers to form gated nanostructures [32, 56, 23], especially with the matured soft lithography technology for polydimethylsiloxane (PDMS) microfluidic stamps [57]. It is worth mentioning that the dielectric layer under the gate should be thin enough to enhance the coupling between the gating voltage and the nanochannel, yet thick enough to minimize the dielectric breakdown. Therefore, a high quality of the gate dielectric is much desirable. In addition, by shrinking the lateral dimensions of the 2D nanoslit structure, a 1D nanotube structure can also be achieved in a similar process. For example, Vermesh *et al* used the

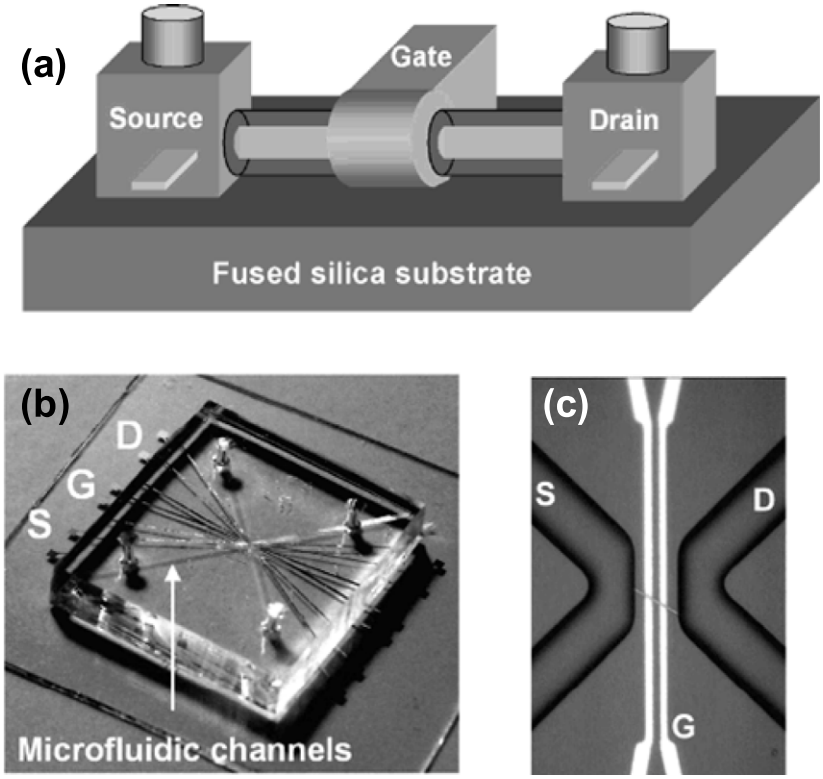

Figure 5. Gated nanochannels with a single silica nanotube harvested from the templated method. (a) Schematic of the gated nanochannel structure; (b) a fully assembled device; (c) a microscopy image showing the device structures. (Reprinted with permission from [55]. Copyright 2006 American Chemical Society.)

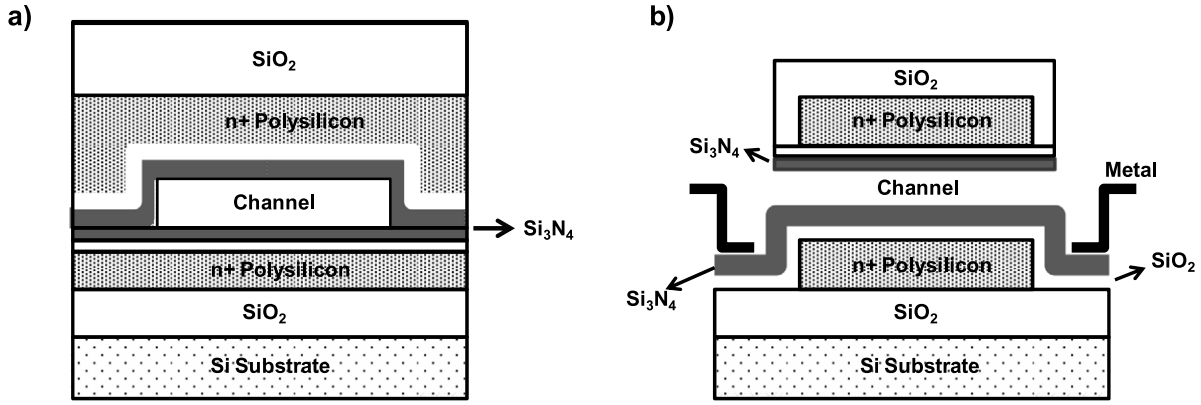

Figure 6. CMOS compatible method with sacrificial layer etching to form the gated nanochannel structure. (a), (b) shows the cross section along the width and along the length of the nanochannel, respectively. (Reprinted with permission from [30]. Copyright 1992 The Electrochemical Society.)

superlattice nanowire pattern transfer (SNAP) technique [58] to form an array of 1D silica nanochannels with 20 nm × 30 nm cross section [59].

One of the key steps in the sacrificial layer based technique with the PDMS microfluidic stamps as interfaces is the sequence of the bonding process and the etching process.

3.2.1.1. 'Etch followed by bond' approach. The conventional method etches the sacrificial layer first and then integrates the nanochannel device with a microfluidic interface to form a functional device [60, 61, 27]. In this approach, the as-fabricated devices are firstly exposed to the etching solutions or gases. After the sacrificial layer is etched away, the device is then rinsed with de-ionized (DI) water and dried in an oven. After that, the surface of both the device and the PDMS stamp are treated with oxygen plasma and they are bonded together. It is during this bonding process that a certain pressure is needed to press these two pieces together. This process is prone to inducing the collapse of the nanochannel [23]. The reasons for the nanochannel collapse may come from two factors, (1) capillary forces in the drying process, and (2) pressure exerted during the PDMS bonding process.

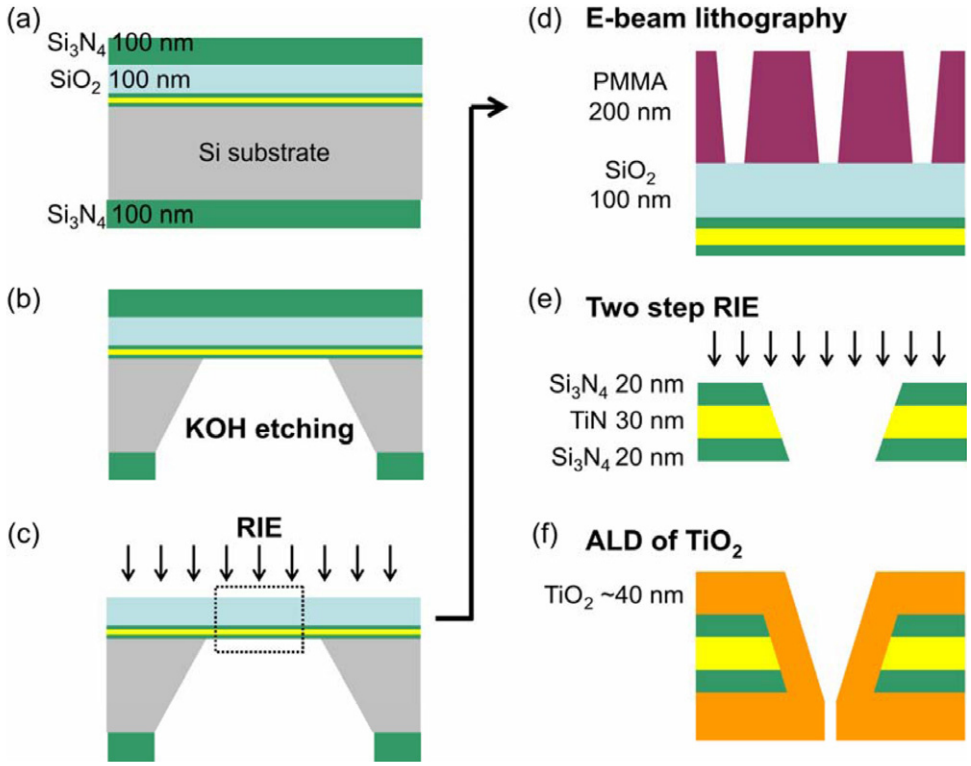

Figure 7. The process flow for the gated nanopore fabrication. Advanced technologies using e-beam lithography and subsequent conformal ALD coating can generate multiple gated nanopore structures with sub-10 nm diameters. (Reprinted with permission from [33]. Copyright 2009 American Chemical Society.)

3.2.1.2. 'Bond followed by etch' approach. To overcome the collapse problem encountered in the 'etch followed by bond' approach, a new scheme was developed by our group to remove the sacrificial layer [23]. The as-fabricated device and the PDMS stamp are firstly treated with oxygen plasma and bonded together. Then the etchant solution is pumped to diffusively etch the embedded sacrificial layer *in situ*. After the etching process is completed, DI water is flushed along the microchannels to rinse the channel. Since there is neither the drying process nor the external pressure applied, the 'bond followed by etch' scheme completely avoids the nanochannel collapse problem.

3.2.2. Gated 0D nanochannels (nanopores). Other than the 2D nanoslit and 1D nanotube structures, nanopores can be deemed as a 0D nanochannel. Nanopore structures have found wide applications in single molecule analysis, including next generation DNA sequencing [62–64, 2]. Gated nanopore structures can also be fabricated using advanced CMOS technologies. For example, Nam *et al* used e-beam lithography and atomic layer deposition (ALD) processes to generate gated nanopore structures [33]. Using a suspended membrane consisting of a metallic TiN layer sandwiched by Si_3N_4 (figures 7(a)–(c)), e-beam lithography and reactive ion etching (RIE) processes are used to generate nanopores with sizes of 70–80 nm (figures 7(d) and (e)). An ALD process is thereafter used to conformally shrink the pore size to sub-10 nm (figure 7(f)). The self-limiting process of the precursor molecules allows a wide process window for uniform nanopore structures [33].

4. Applications

4.1. Field effect controlled electro-osmosis

When a tangential electric field is applied along the channel surface, electro-osmotic flow (EOF) will develop due to the viscous coupling between the ions in the diffuse layer and the bulk liquid. The electro-osmotic velocity v_{EO} is highly dependent on the ζ potential at the channel surface. As a result, by applying a gating voltage over an integrated thin insulator, the EOF can be accelerated, slowed down, or even reversed by modulating the ζ potential (figure 8). The principle has been thoroughly demonstrated in fused silica capillaries [65, 66], in micro-capillaries [7, 67], and in nanochannels [68, 69, 37]. Though the principle has been successfully demonstrated, there are still several difficulties that need to be solved before this technology can be put into real commercial systems. These difficulties include: (1) poor control at pH values where the surface charge density is high, which will overwhelm the influence of the external voltage-induced charges in the EDL [70, 69], and (2) gas formation by electrolysis at the electrodes that provide the longitudinal electric field [71]. Nevertheless, this direct field effect control over the liquid flow in both microchannels and nanochannels opens up wide opportunities for various lab-on-a-chip applications.

4.2. Ionic field effect transistor

In the same way electrons/holes being modulated in the MOSFET device by an external electric field, cation and

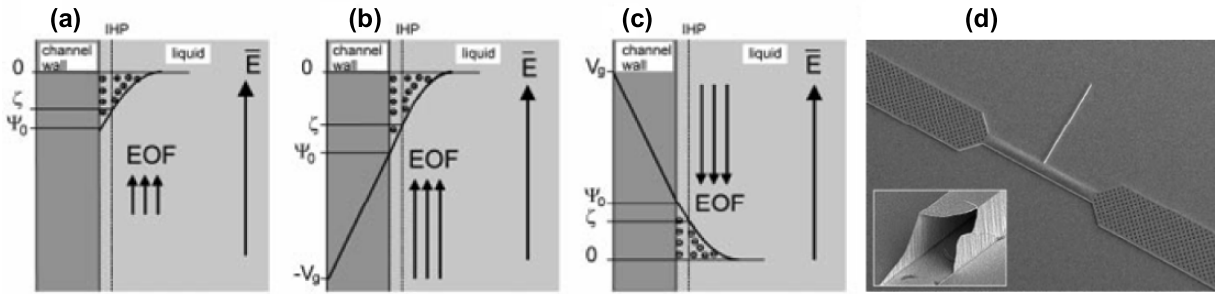

Figure 8. Field effect controlled electro-osmosis in silica channels. (a) Illustration of the development of the ζ potential and EOF at the interface, (b) applying a negative gating voltage will accelerate the EOF flow, (c) the ζ potential as well as the EOF can be reversed by applying a large positive gating voltage, (d) SEM image of the gated structure for field effect control over electro-osmosis flow. (Reprinted with permission from [7]. Copyright 1999 AAAS.)

anion population in the nanochannels can be manipulated in a similar fashion with an ionic field effect transistor. This is because the electron/hole and the cation/anion shares very similar physics. For example, the charge distribution at low concentrations for both of them obeys the Boltzmann relation. However, they also have very notable differences, e.g., ions move much more slowly than electrons/holes and cations and anions cannot recombine. So far, researchers have used the similarity between the nanofluidic and semiconductor system to achieve direct electric field–charge interactions in nanochannels. While field effect controlled electro-osmosis can be realized in both microscale and nanoscale channels, field effect controlled ionic modulation can only be achieved in nanochannels where the channel size is close to or even smaller than the Debye length.

The main purposes for direct field effect control over charged species in nanochannels are twofold. The first is to investigate the fundamental physico-chemical process in this novel system. The second is to realize a precise and active control over ionic species such as protons as well as important biomolecules such as proteins and nucleotides.

4.2.1. Ionic switch. The first experimental results of an ionic field effect transistor were demonstrated by Gajar and Geis in 1992 [30]. The devices they built have nanochannels about 88 nm in height and 300–900 μm in length. They investigated both the steady-state and transient responses of their ionic FET devices. However, it is found that the response of the ionic FET to a step voltage in the gate terminal is quite slow. This is mainly due to two reasons. The first is the large geometries of the nanochannel and the second is the existence of processes other than ambipolar diffusion.

In 2004, theoretical modeling of the ionic transport in silica nanotubes revived research interest in ionic FET devices [72]. Fan *et al* experimentally demonstrated field effect modulation of ion transport using gated silica nanotubes [31]. Using KCl as the testing solution, they found that as the gate voltage varies from -20 to $+20$ V, the ionic conductance decreases monotonically from 105 pS down to 45 pS, due to depletion of cations (K^+) under the applied electric field, which shows a typical p-type transistor behavior (figure 9). Since then, various field effect ionic transistors have been reported [73].

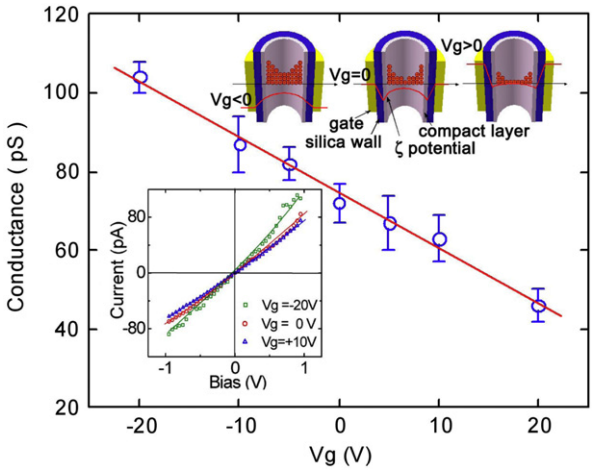

Figure 9. Ionic conductance as a function of gate voltage in gated nanochannels filled with KCl. The cation ion concentration and thus the conductance can be modulated by a gating voltage. Top inset schematically shows field effect modulation of electrical potential profiles. Bottom inset shows selected I–V curves. (Reprinted with permission from [31]. Copyright 2005 American Physical Society.)

Ionic switches can also be realized in gated nanopore or nanopore array structures [34, 33]. Using multiple nanopore structures with sub-10 nm diameters and TiO_2 as dielectric material, Nam *et al* showed that the ionic conductivity of the nanopore can be modulated by a gating voltage [33]. A p-type I_d–V_g characteristic is also observed, which suggests the majority carriers are cations (figure 10).

To change the majority carries in gated nanochannels, chemical modifications to the nanochannel wall can be utilized. For example, Fan *et al* used aminosilane chemistry to modify the surface charge polarities [31]. As shown in figure 11, one day of (3-aminopropyl)triethoxylsilane (APTES) functionalization did not change the surface charge polarity (still p-type behavior), but led to a greatly reduced ionic conductance and a more pronounced gating effect due to the reduced surface charge densities (figure 11(d)). Two days of APTES functionalization resulted in ambipolar transport behavior (figure 11(e)), which indicates a quasi-neutral surface. Four days of APTES treatment converted the as-made p-type

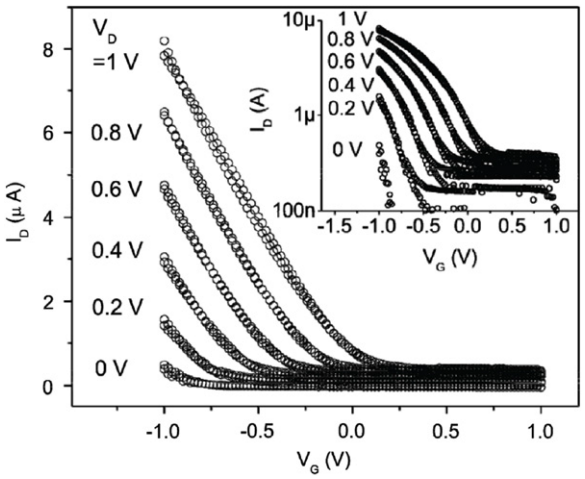

Figure 10. I_d–V_g plot when V_d is between 0 and 1 V. P-type unipolar behaviors were observed, which means that the majority carriers are positive K^+ ions. Inset is the I_d–V_g on a semi-log scale. (Reprinted with permission from [33]. Copyright 2009 American Chemical Society.)

ionic FET into a n-type ionic FET (figure 11). The chemical modification at the surface is equivalent to doping technology in semiconductors.

Even though ionic FETs have been proposed for logic operations [74], it is the authors' opinion that ionic devices may be very hard to implement for logic circuits, if not at all impossible. This is because ions have a mobility that is three orders of magnitude lower than electrons and holes, which makes logic operation using ionic circuits very unpractical.

The main challenges in realizing an effective and reliable ionic switch device using gated nanochannels include the following: (1) A high surface charge density on nanochannel walls makes the electrostatic gating very inefficient, (2) the buffering capacity of the chemically reactive surface overwhelms the electrostatic modulation (section 2.2.4), (3) the leakage current through the gate dielectric overwhelms the weak ionic current through the nanochannel, and (4) control over the ionic population at high concentrations requires a much smaller nanochannel size. To overcome the first three problems, a thorough search and detailing of the dielectric materials are of high importance. An ideal dielectric material should be hydrophilic, chemically inert, impermeable to small ions such as protons, and with a neutral surface. To solve the fourth challenge, reliable techniques to fabricate nanochannels with sizes below 10 nm [24] or intrinsic materials with smaller channel sizes [29] are desirable.

4.2.2. Molecular switch.

4.2.2.1. DNA. Since biomolecules usually have multivalent charges, field effect control over the molecule transport in nanochannels can be more effective than monovalent ions. It has been experimentally observed that the fluorescence intensity of 30-base fluorescently labeled single-stranded DNA (ssDNA) in a 1 mM KCL solution could be increased by

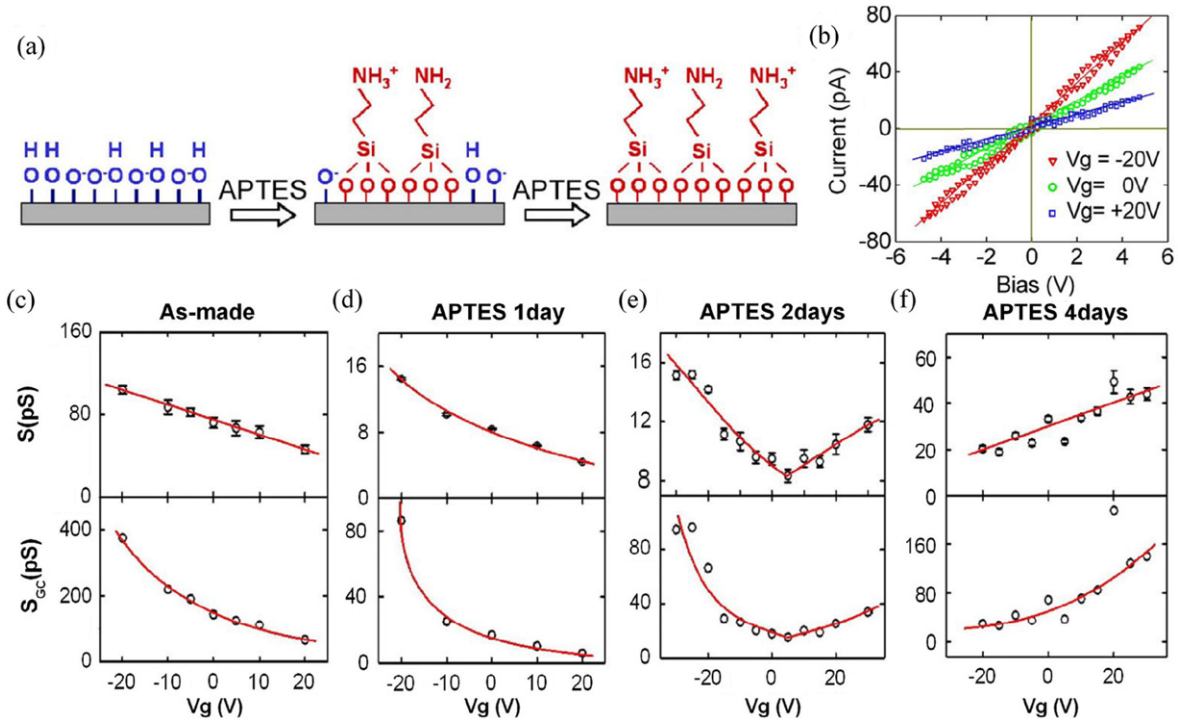

Figure 11. Surface charge control by chemical modification. (a) Schematic of APTES modification to a SiO_2 surface, (b) selected I–V curves for the ionic FET device after one day of APTES treatment. (c)–(f) Measured ionic conductance (S) and the effective conductance at gate controlled regions (S_{GC}) as a function of gate voltages for as-made and functionalized devices. It is clear that surface modification can greatly affect the field effect control over the ions in the nanochannels. (Reprinted with permission from [31]. Copyright 2005 American Physical Society.)

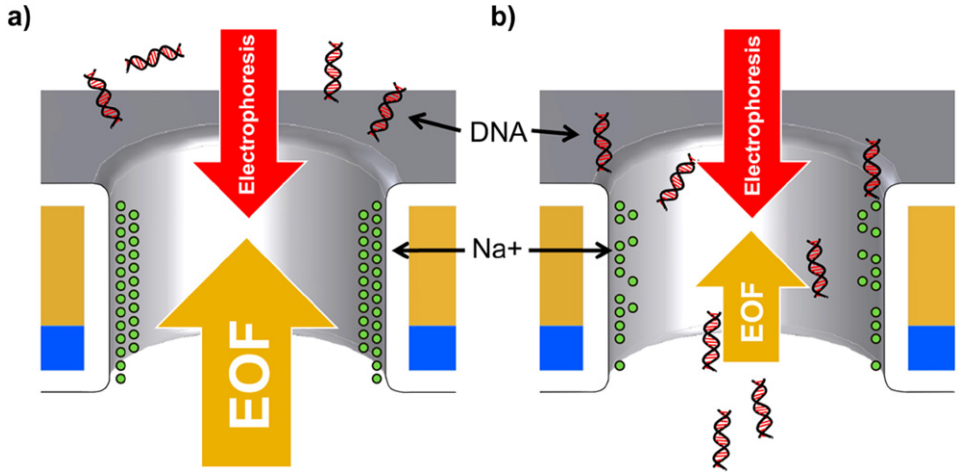

Figure 12. Schematic of the EOF barrier-limited operation of a DNA switch. (a) EOF overwhelms the EP when the gating voltage is low. DNAs are rejected from entering the pore. (b) A high gating voltage reduces the EOF due to the reduced Na^+ in the diffuse layer (section 4.1). DNAs are accepted to pass through the nanopore. (Reprinted with permission from [76]. Copyright 2012 American Chemical Society.)

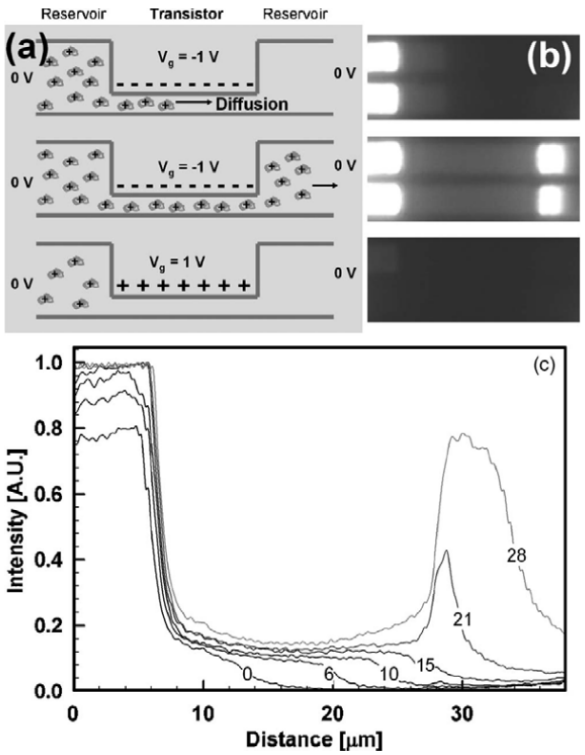

Figure 13. Field effect controlled protein switch. (a) Schematic showing diffusion of avidin when applying gating voltages of different polarities. (b) Corresponding fluorescence images. (c) Fluorescence intensity along the nanochannel showing the diffusion of avidin along the channel. Numbers on the line plots denote time in minutes. (Reprinted with permission from [3]. Copyright 2006 American Institute of Physics.)

six times in 2D nanoslits, which is ascribed by the electrostatic interactions between the gating voltage and DNA molecules [32].

The field effect regulation of DNA translocation through a 0D nanopore has been simulated using a continuum model, composed of the coupled Poisson–Nernst–Planck equations and Navier–Stokes equations [75]. It is found that both electro-osmotic flow (EOF) and electrostatic interactions arising from the field effect control can effectively regulate the DNA translocation through a nanopore. Recently, Paik *et al* demonstrated a gated nanopore structure that is capable of reversibly altering the rate of DNA capture by over three orders of magnitude [76]. They ascribed this extremely large modulation ratio to the counter-balance between the electrophoresis (EP) and the EOF (figure 12), rather than pure electrostatic interactions between the gating voltage and the DNA molecules. As a result, a clear physical picture of the gated DNA translocation through the nanopore is still lacking. More efforts are required to unambiguously show the DNA regulation mechanism in gate nanochannel structures.

4.2.2.2. Protein. Field effect control of protein transport in nanochannels is much more complex than in DNA. The surface of proteins is usually very active and the same protein can have various conformations under different microenvironments. The ideal system for field effect control over protein transport in nanochannels is a hydrophilic channel with a neutral surface, and a charged, stable protein. Very few works in the existing literature have demonstrated field effect gated protein transport in nanochannels. Karnik *et al* showed field control over the protein avidin in a surface modified silica nanochannel [3]. As shown in figure 13, a fluorescent front was seen to diffuse out from the reservoir when the gating voltage was −1 V. Because avidin is positively charged, the concentration will be enhanced by the application of a negative gate voltage. This front eventually reached the central reservoir and started filling it. This is a slow diffusion process (∼30 min) since there is no horizontal driving force across the nanochannels. The extracted diffusivity of avidin is found to be two orders of magnitude smaller than typical protein diffusivities in bulk solutions, which suggests that interactions within the channels dramatically decreased the diffusivity of avidin.

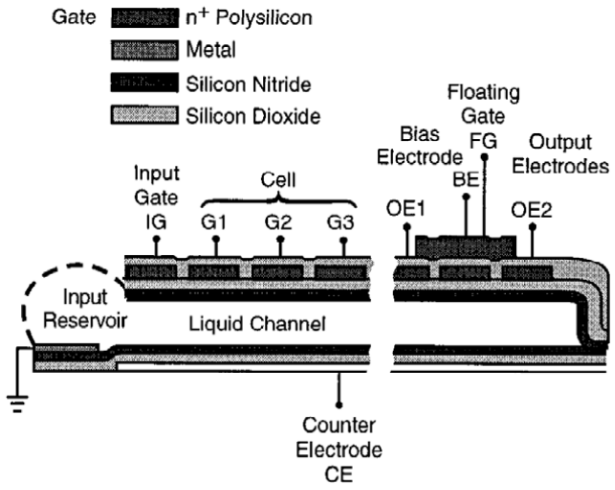

Figure 14. Schematic of the chemical CCD device, showing an array of electrodes with a three-phase electrode biasing design. The design and the operation of this device are very similar to a silicon CCD device. (Reprinted with permission from [77]. Copyright 1997 American Vacuum Society.)

When applying the gate voltage as +1 V, the fluorescence intensity decreased, indicating that the avidin had been repelled out of the gated region. Therefore, a successful electronic protein switch was demonstrated.

4.3. Ionic charge coupled device

Stern *et al* proposed an interesting gated nanochannel structure, named as the chemical charge coupled device (CCD) [77]. It is an extension of the ionic FET to multiple-gate structures. It is expected to have the capability of separating ions according to their mobility. The proposed chemical CCD sensor is similar to the silicon CCD device in both the design and operating principles. The chemical CCD structure, shown in figure 14, consists of a series of gating electrodes and a bottom counter electrode that are insulated from the nanochannels. It is expected that ions will be drawn into the nanochannels by sequentially applying voltages to the gating electrodes.

Once a packet of cation ions is formed in the channel, the ionic constituents can be separated according to their diffusion coefficients and the clocking rate, or stepping frequency of the gating voltage. Ion separation appears because it takes a longer time for ions with low diffusion coefficients to move between the regions controlled by adjacent gating electrodes than ions with higher diffusion coefficients. If the stepping frequency does not allow sufficient time for a given set of ion constituents to diffuse between adjacent electrode regions, then the ion flux in the nanochannel will be reduced for that constituent. Although Stern *et al* showed no experimental results on ion separation, the chemical CCD concept represents a very intriguing device structure that may have important applications. The main difficulty in realizing such a device largely lies in the reliable fabrication of the gated nanochannel with multiple-gate electrodes.

4.4. Ionic field effect reconfigurable diode

In ionic FETs [30–32, 3, 29, 33, 34], only the amount of ions/molecules is regulated. A directional control, which is a typical diode property, is lacking in ionic FETs. Analogous to a solid-state semiconductor diode for regulating the flow of electrons/holes in one preferential direction, nanofluidic diodes are also being developed to achieve rectified ionic transport—ions favorably move in one direction and are inhibited in the opposite direction. The topic of two-terminal nanofluidic diode devices was extensively reviewed recently by Cheng *et al* [78]. Such a rectification effect is of great importance due to its relevance to biological ion channels [79].

Several engineered nanofluidic platforms based on nanopores and nanochannels were reported to produce ionic current rectification by symmetry breaking [78] in geometries [80–83], surface charge distributions (either intrinsic material properties [56, 84] or chemically modified properties [27, 28]), bath concentrations [60], or a combination of these, for example, by positively and negatively patterning charged regions in conical nanopores [85]. Nevertheless, it has not been possible to change the predefined rectifying properties obtained by these approaches once the devices are made. Although several externally tunable methods have been proposed so far, most of them aim to alter the nanochannel wall property by introducing external chemical stimuli, for example, hydronium ions (pH) [86–88], enzymes [89] and polyvalent cations [90]. All these methods require changing the native environment of the solution being transported.

Since an electric field normal to the nanochannel walls is able to enhance or diminish the ionic concentrations near the surface *in situ* [30–32, 3, 29, 33, 34], our group proposed and demonstrated a field effect reconfigurable diode (FERD) by asymmetrically modulating the cation/anion ratios along the nanochannel [23].

The schematic structure of FERD device and the experimental setup is illustrated in figure 15(a). The FERD has a similar structure to ionic FETs, yet with a critical difference that the gate electrode of FERD is *asymmetrically* located near one of the microfluidic reservoirs. We found that the I–V characteristic along the nanochannel is highly dependent on the gating voltage as well as the location of the gate electrode. As shown in figures 15(a) and (b), a clear gate voltage controlled rectifying property is observed in the FERD device with *asymmetrically* located gate electrodes (figure 15(a)). In contrast, the control device (with *symmetrically* placed gate electrodes) shows no rectifying property, though the conductance can be modulated by the gating voltage, which is a typical ionic FET characteristic (figures 15(c) and (d)).

Moreover, by independently creating separated p and n regions along the nanochannel, the field effect regulated rectification property can be enhanced (figures 16(a) and (b)). In the split-gate version of FERD devices, the preferential ionic current direction as well as the rectification degree can be modulated much more pronouncedly (figure 16(c)), as compared to the data shown in figure 15(b).

FERD device represents a fundamentally novel system and may function as the building block to create on-demand, reconfigurable, large-scale integrated nanofluidic circuits for

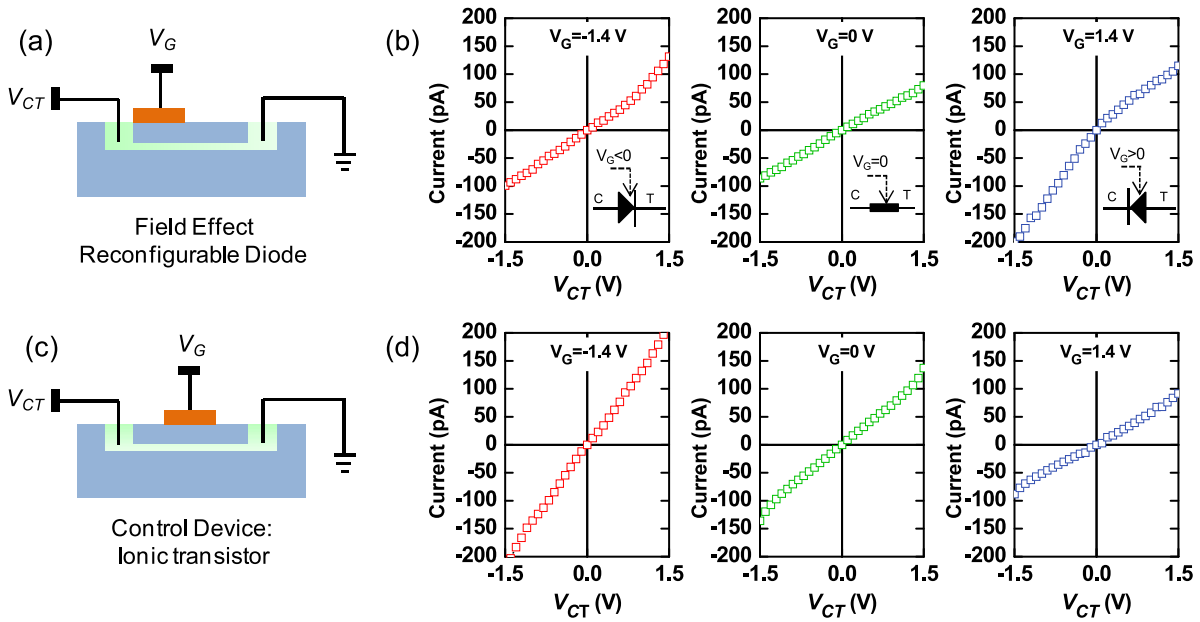

Figure 15. Current–voltage (I–V) curves for the FERD devices (top row) as well as the control devices (bottom row) with different gate voltage (V_G) polarities. (a) Testing configurations for the FERD device. (b) I–V curves for FERD devices ($W = 2\ \mu\text{m} \times 11$, $L = 100\ \mu\text{m}$, $H = 20$ nm) using a 100 μM KCl solution. (c) Testing configurations for the control transistor device. (d) I–V curves for the control device ($W = 3\ \mu\text{m} \times 11$, $L = 100\ \mu\text{m}$, $H = 20$ nm) using a 100 μM KCl solution.

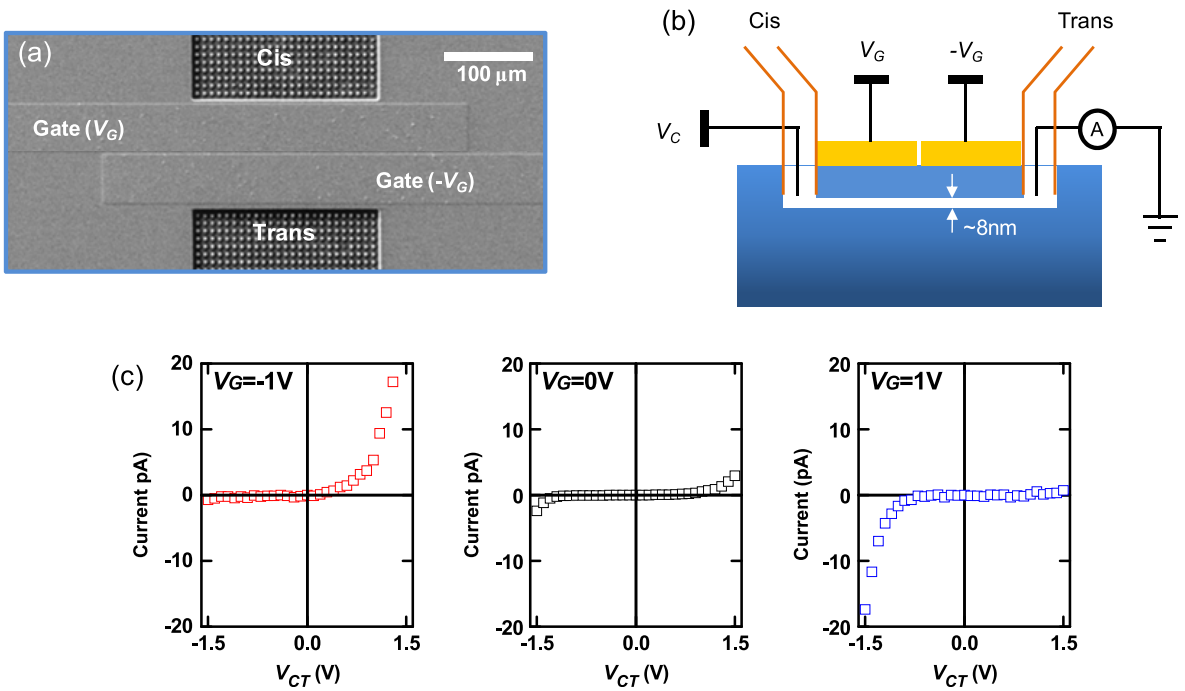

Figure 16. (a) SEM image of the dual split-gate FERD devices ($W = 1\ \mu\text{m} \times 11$, $L = 116\ \mu\text{m}$, $H = 8$ nm). The scale bar is 100 μm. The nanochannel wall is chemically modified to be less charged and hydrophilic. The separation between the two gates is 4 μm. (b) Testing configurations for the dual gate FERD device. (c) Typical I_{ct}–V_{ct} curves at different gate voltages (−1 V, 0 V, +1 V) for a given ionic concentration (1 mM).

digitally programmed manipulation of biomolecules such as polynucleotides and proteins. It is worth mentioning that this general concept could conceivably be applied to similar thin-body solid-state devices (e.g., silicon-on-insulator or semiconducting nanowire).

4.5. Field effect enhanced energy conversion

Nanochannels can be engaged in the energy conversion in two ways. The first is pressure driven energy conversion (streaming potential) [91, 6, 92, 93], and the second is salinity gradient

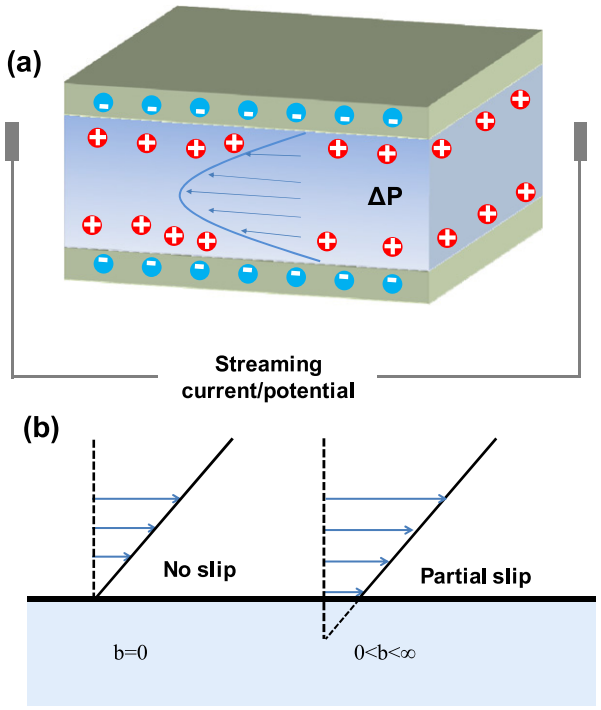

Figure 17. (a) Pressure driven energy conversion (streaming current/potential), (b) slip flow past a stationary surface. Slip and no-slip boundary conditions are shown. The slip length b is indicated for each case.

power by reverse electrodialysis [94, 95]. The efficiency of both energy conversion methods can be enhanced by the field effect.

4.5.1. Field effect enhanced pressure driven energy conversion. A pressure driven flow through a microfluidic or nanofluidic channel will bring the ions in the diffuse layer downstream, thus generating an electrical current (figure 17(a)). When this so-called streaming current is driven through an external load, electrical energy is harvested from the fluidic system. The energy conversion efficiency is expected to be the highest in nanochannels because of the double layer overlap [6]. It is also found that the power generation efficiency is greatly correlated with the slip/no-slip boundary conditions. Theoretical calculations using Poisson–Boltzmann (PB) theory for EDL and Navier–Stokes for fluid flow, have estimated a maximal energy conversion efficiency around 15% with no-slip boundary conditions [96, 6, 97] and around 30% with slip boundary conditions [98, 99].

The reason why the no-slip boundary condition has a lower energy conversion efficiency is because there is no fluid or ion flow at the surface, where the counter-ion concentration is the highest (figure 17(b)). The no-slip boundary condition is most common in real nanochannels, which severely limit the energy conversion efficiency in the experiment.

If the no-slip boundary condition in hydrophilic nanochannels could be surmounted, greatly enhanced streaming currents and energy conversion efficiencies would be possible, making energy conversion in such systems far more feasible. In order to achieve this, Vermesh *et al* [59] has showed that the slip length in an array of 20 nm wide, 20 μm long SiO_2 nanochannels can be modulated within a range of 2–10 nm by gating voltages (figure 18). The ability to tune the slip length by gating voltages is very encouraging from the point of view of energy conversion. However, more experiments are required to thoroughly test this hypothesis.

4.5.2. Field effect modulated salinity gradient power generation. Reverse electrodialysis (RED) is a technology used to generate energy by mixing aqueous streams with different salinity. The key components in a RED system are the ion exchange membranes with ion selectivity. This technology was extensively studied in the discipline of membrane sciences [94] and recently in engineered nanochannels [95, 5]. Kim *et al* recently reported a power density of 7.7 W m^{-2} and efficiency of 31% in engineered silica nanochannels [95]. Power generation from concentration gradients in nanochannels can be useful in a variety of applications, including micro-batteries and micro-power generators. This energy conversion approach shares the same principle as the membrane potential in cells, where the concentration gradient and the ionic selectivity of the nanochannel are two key factors that determine the membrane potential.

Inspired by the action potential generation behavior in voltage gated ion channels (figure 19(a)), our group demonstrated a gated nanochannel structure with tunable potential that comes from a salinity gradient [100]. The three-terminal device we demonstrated is structurally similar to an ionic FET device [30, 32], except that the longitudinal driving force is a concentration gradient instead of a potential gradient (figures 19(b)–(d)). The orthogonal electric field produced by the gating voltage is expected to mediate the ionic selectivity in the nanochannel through electrostatic interactions.

The *steady-state* potential ΔV_{ct} developed across ion-selective nanochannels can be described by [101]

$$\Delta V_{ct} = (2t^{+} - 1)\frac{RT}{F}\ln\frac{[trans]}{[cis]}, \qquad (21)$$

where R, T, and F are universal gas constant, absolute temperature and Faraday constant, respectively. $[x]$ denotes the salt concentration in the x side ($x = cis$ or $trans$). t^{+} is the cation transport number, that is, the ratio of cations to all ions in the channel.

With increasing gating voltage, V_s, cation/anion concentration will be diminished/enhanced accordingly. Therefore t^{+} is a monotonically decreasing function of V_s, bounded within 0 and 1 (figure 20(a)). By modulating the steady-state t^{+} by a gating voltage V_s, it is able to modulate the salinity gradient potential ΔV_{ct}.

Figure 20(b) exhibits the steady-state ΔV_{ct} as a function of V_s at low salt concentration conditions, with the device of a reduced surface charge density (σ_s) as -0.28 mC m^{-2}. Figure 20(b) reveals a set of informative features as predicted by equation (21). First of all, no potential appears if there is no cis–$trans$ concentration gradient. When $[cis] < [trans]$, ΔV_{ct} exhibits the same trend as t^{+}, while for $[cis] > [trans]$, the trend between ΔV_{ct} and t^{+} becomes opposite. Moreover, ΔV_{ct} can be modulated into different polarities, thanks to $t^{+} > 1/2$ when $V_s = -1.5$ V and $t^{+} < 1/2$ when $V_s = 1.5$ V.

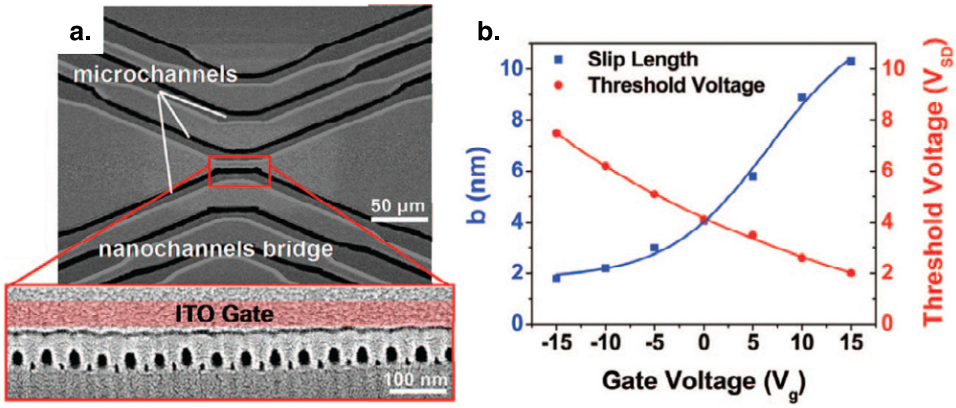

Figure 18. Field effect induced slip in nanochannels. (a) SEM of the gated nanochannel structures. The six V-shaped structures are microfluidic channels. The two opposing microchannels in the central region of the image are bridged by the 20 μm long nanochannel array. The magnified image shows the cross-section SEM view of a few of the (20 nm wide $\times$ 30 nm high) nanochannels, with the position of the ITO gate electrode indicated. (b) Dependence of the slip length and threshold voltage (above which slip occurs) with respect to the gate voltage. (Reprinted with permission from [59]. Copyright 2009 American Chemical Society.)

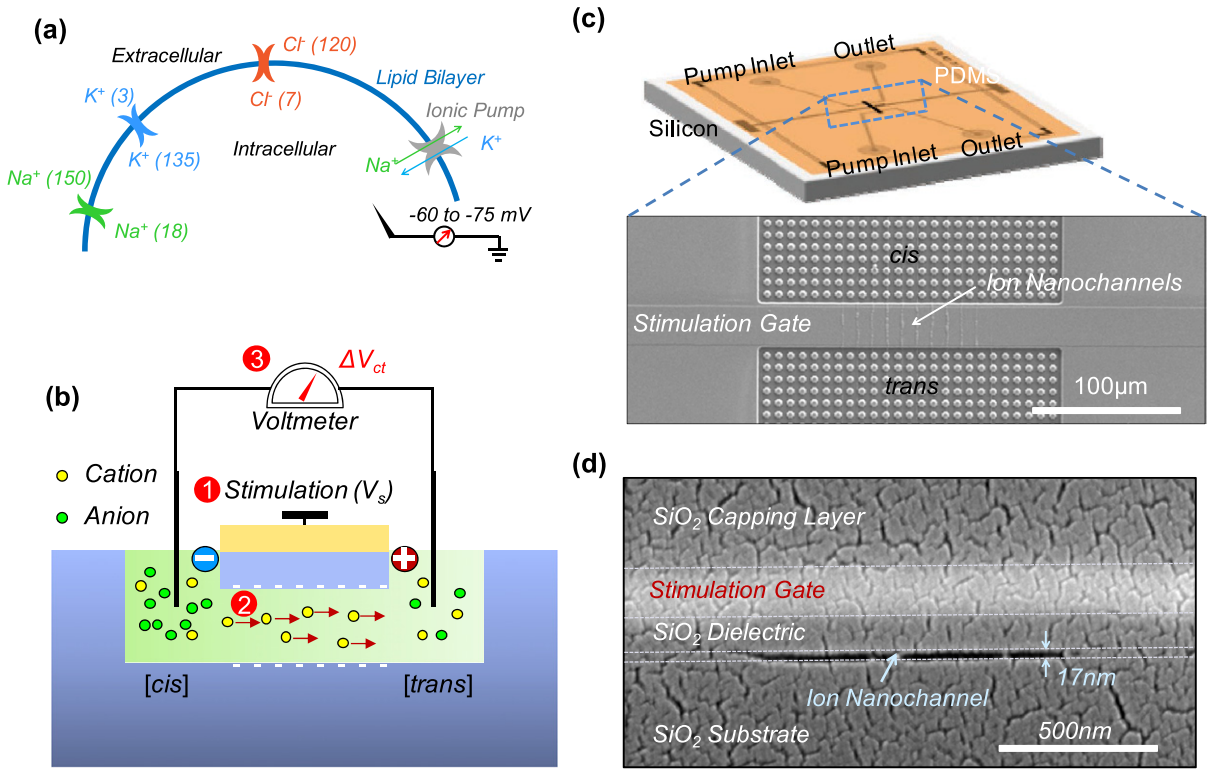

Figure 19. Device principles and experimental setup for field effect modulated salinity gradient power generation. (a) Schematics of typical intracellular and extracellular fluids with different ionic concentrations. The cell is in a charge polarization state due to selective ion transport in the ion channels, bringing about a resting membrane potential. (b) Cross-section sketch of the device. A gating voltage normal to the nanochannel walls (step 1) alters the ion selectivity in the nanochannel (step 2), resulting in a modulated transmembrane potential (ΔV_{ct}) (step 3). (c) Sketch of the planar layout for the assembled device. (d) Cross-sectional SEM image showing a single nanochannel with a height of 17 nm and a width of 1 μm. (Reprinted with permission from [100]. Copyright 2012 American Chemical Society.)

The quasi-static ΔV_{ct} modulation is also salt concentration dependent. The red squares in figure 20(c) show the steady-state ΔV_{ct}–V_s relationships for $[trans]$ ranging from 10 μM to 1 M and $[cis]$ fixed at 10 μM, using the same device of $\sigma_s = -0.28$ mC m^{-2}. As can be seen, when increasing the *trans* concentration, it becomes harder and harder to experimentally access the V_{sp} and V_{sn} voltages because of the smaller Debye length compared with the nanochannel dimensions, leading to a situation where creating a unipolar ion environment becomes impossible.

Another factor that affects the modulation behavior is the surface charge density on the nanochannel walls. The blue triangles in figure 20(c) present the results for the device with $\sigma_s = -1.6$ mC m^{-2}. With such a high negative

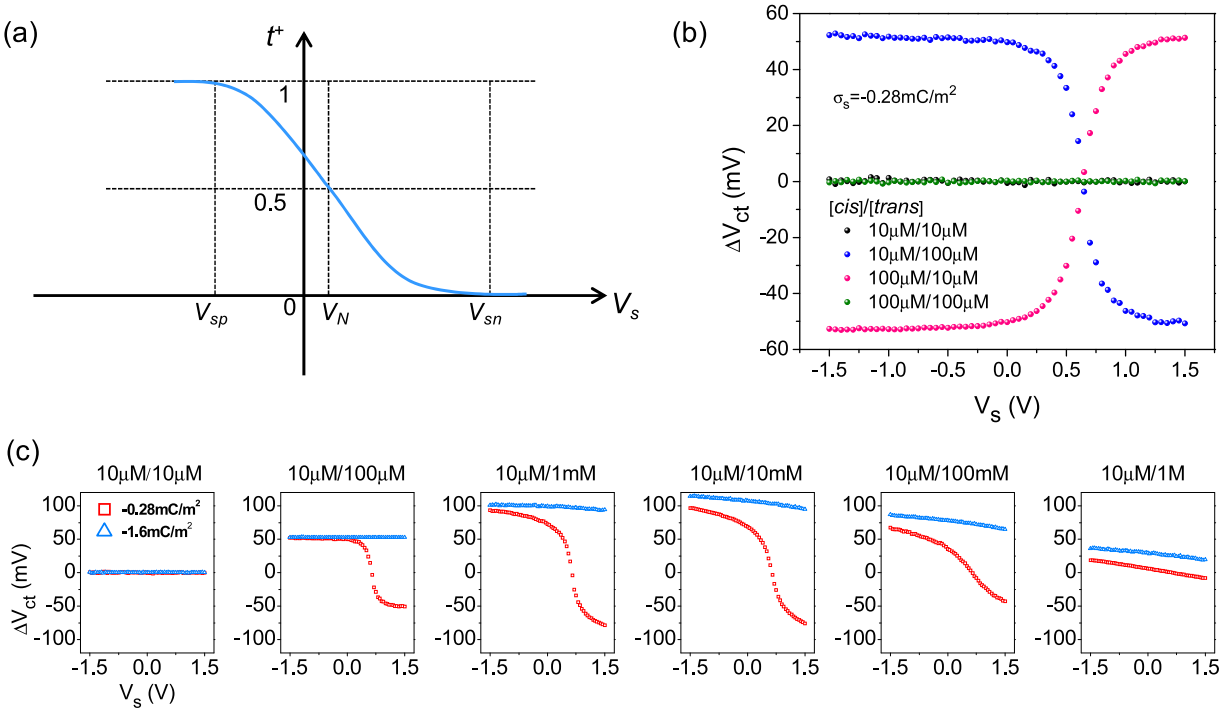

Figure 20. Field effect modulated salinity gradient potential by gating voltages. (a) Cation transport number t^+ as a function of the gating voltage V_s. V_{sp}, V_N and V_{sn} denotes the voltages at which the nanochannel is pure cation selectivity, no selectivity and pure cation selectivity, respectively. (b) Results in the low salt concentration regime with the device of $\sigma_s = -0.28$ mC m^{-2}. (c) Salt concentration and the surface charge dependence of the modulation behavior. (Reprinted with permission from [100]. Copyright 2012 American Chemical Society.)

surface charge, the nanochannel is dominated by cations ($t^+ > 1/2$), since V_s within ± 1.5 V is too small to reverse the charge polarity (the smallest absolute V_s required to reverse is approximately $2\sigma_s d_{ox}/\varepsilon_0\varepsilon_{ox}$, which is around 4.7 V for $\sigma_s = -1.6$ mC m^{-2} and $d_{ox} = 50$ nm). As a result, ΔV_{ct} can only be modulated within the positive range for $[trans] > [cis]$ (equation (21)). The maximum modulation range of ΔV_{ct} in $\sigma_s = -1.6$ mC m^{-2} is much less than that in $\sigma_s = -0.28$ mC m^{-2}, when V_s ranges from -1.5 to 1.5 V. This inefficient modulation is also due to the fact that an inherent high surface charge density resembles high densities of surface states in a FET, making electrostatic modulation over the ionic population (and thus t^+) difficult [23]. Therefore, a nanochannel with lower or neutral surface charge density is favorable for an efficient modulation of the salinity gradient potential.

5. Conclusions and perspectives

Nanochannels offer a unique opportunity for both fundamental sciences and technological applications. There are enormously intriguing physical and chemical processes in the nanometer-sized geometries, which could be exploited for chemical, biological, and electrochemical applications.

First, active control of the ion and molecule transport in voltage gated nanochannels provides the possibility to seamlessly integrate wet ionic devices with dry electronics, enabling long-sought electronic–biological interfaces that presently suffer from surface chemistry reproducibility issues. This kind of system can function as the building block to create on-demand, large-scale integrated nanofluidic circuits for digitally programmed manipulation of important ions such as protons and biomolecules, such as polynucleotides and proteins, which could potentially be a well-controlled electronic cellular interface. In addition, all the electronic transport functions described here do not involve reactions, and the engineering of internal reactions could potentially create non-trivial nonlinear characteristics (such as negative differential resistance) for complex circuit functions, or oscillators.

A second potential application of engineered nanochannels is for separators and concentrators. The obvious low sample throughput of nanochannels can be enhanced by parallel microfabrication strategies discussed in the paper, although applications would probably be limited to analytical and detection purposes instead of large-scale purification.

A third potential application is for enhanced batteries. Enhanced ion transport improves the power density and energy density of batteries. The useful energy density of batteries, including Li-ion rechargeable batteries, is limited by inefficient ion transport. The engineered systems and analysis techniques described in this paper could point to material and structural designs that could dramatically enhance performance.

Finally, the basic transport phenomena in nanochannels, especially in the voltage gated nanochannels, still remains as a topic for current research and will likely produce the most interesting applications. This is because the most complex systems will involve complex and coupled processes including electrostatics, chemical reactions, non-specific wall–ion or

wall–molecule interactions, fluid dynamics, and electrokinetics. An example is that gated DNA and protein transport in nanoscale channels are not totally understood in most experiments.

Moreover, most of the present studies only deal with a simple symmetric monovalent electrolytes because it is a simple physical system that can be easily understood by mean field theory (Poisson–Boltzmann theory). However, real applications may involve multivalent ion species such as Ca^{2+} and Mg^{2+}. The simplified scenario of a mean field theory becomes inadequate because of the strong interactions between multivalent ions. As a matter of fact, the 'charge inversion' phenomenon has been observed in which counter-ions with high valence condense onto the surface and actually reverse the sign of its total charge [102, 103, 90]. Work on multivalent species—and their interactions—are less explored, especially with new analysis techniques.

The theoretical and technological advances in engineered synthetic ionic nanochannels have been considerable over the past decade, and represent new emerging fields of intriguing fundamental science and application. One of the most intriguing challenges is to eventually connect the lessons learned to the first engineered ionic nanochannels, nature's own biological ion channels.

Acknowledgments

WG acknowledges the support from Howard Hughes Medical Institute International Student Research Fellowship. This research was supported as part of the Nanostructures for Electrical Energy Storage, an Energy Frontier Research Center funded by the US Department of Energy, Office of Science, Office of Basic Energy Sciences under Award Number DESC0001160. We also acknowledge the Yale Institute for Nanoscience and Quantum Engineering and NSF MRSEC DMR 1119826.

References

[1] van den Berg A, Craighead H G and Yang P D 2010 From microfluidic applications to nanofluidic phenomena *Chem. Soc. Rev.* **39** 899–900
[2] Branton D *et al* 2008 The potential and challenges of nanopore sequencing *Nature Biotechnol.* **26** 1146–53
[3] Karnik R, Castelino K and Majumdar A 2006 Field-effect control of protein transport in a nanofluidic transistor circuit *Appl. Phys. Lett.* **88** 123114
[4] Kim S J, Ko S H, Kang K H and Han J 2010 Direct seawater desalination by ion concentration polarization *Nature Nanotechnol.* **5** 297–301
[5] Guo W, Cao L X, Xia J C, Nie F Q, Ma W, Xue J M, Song Y L, Zhu D B, Wang Y G and Jiang L 2010 Energy harvesting with single-ion-selective nanopores: a concentration-gradient-driven nanofluidic power source *Adv. Funct. Mater.* **20** 1339–44
[6] van der Heyden F H J, Bonthuis D J, Stein D, Meyer C and Dekker C 2006 Electrokinetic energy conversion efficiency in nanofluidic channels *Nano Lett.* **6** 2232–7
[7] Schasfoort R B M, Schlautmann S, Hendrikse L and van den Berg A 1999 Field-effect flow control for microfabricated fluidic networks *Science* **286** 942–5
[8] Abgrall P and Nguyen N T 2008 Nanofluidic devices and their applications *Anal. Chem.* **80** 2326–41
[9] Prakash S, Piruska A, Gatimu E N, Bohn P W, Sweedler J V and Shannon M A 2008 Nanofluidics: systems and applications *IEEE Sensors J.* **8** 441–50
[10] Sparreboom W, van den Berg A and Eijkel J C T 2009 Principles and applications of nanofluidic transport *Nature Nanotechnol.* **4** 713–20
[11] Schoch R B, Han J Y and Renaud P 2008 Transport phenomena in nanofluidics *Rev. Mod. Phys.* **80** 839–83
[12] French R J and Zamponi G W 2005 Voltage-gated sodium and calcium channels in nerve, muscle, and heart *IEEE Trans. Nanobiosci.* **4** 58–69
[13] Sigworth F J 2003 Life's transistors *Nature* **423** 21–2
[14] Morgan H and Green N G 2002 *AC Electrokinetic: Colloids and Nanoparticles* (Baldock: Research Studies Press)
[15] Debye P and Hückel E 1923 Zur theorie der elektrolyte. I. Gefrierpunktserniedrigung und verwandte Erscheinungen *Phys. Z.* **24** 185–206
[16] Gouy G 1910 Sur la constitution de la charge électrique à la surface d'un électrolyte *J. Phys. Théor. Appl.* **9** 457–68
[17] Chapman D L 1913 A contribution to the theory of electrocapillarity *Phil. Mag. J. Sci.* **25** 475–81
[18] Grahame D C 1947 The electrical double layer and the theory of electrocapillarity *Chem. Rev.* **41** 441–501
[19] Guan W H, Rajan N K, Duan X X and Reed M A 2013 Quantitative probing of surface charges at dielectric-electrolyte interfaces *Lab Chip* **13** 1431–6
[20] Lyklema J 1995 *Fundamentals of Interface and Colloid Science: Solid–Liquid Interfaces* (New York: Academic)
[21] Hunter R J 1988 *Zeta Potential in Colloid Science: Principles and Applications* (New York: Academic)
[22] Schoch R B and Renaud P 2005 Ion transport through nanoslits dominated by the effective surface charge *Appl. Phys. Lett.* **86** 253111
[23] Guan W H, Fan R and Reed M A 2011 Field-effect reconfigurable nanofluidic ionic diodes *Nature Commun.* **2** 506
[24] Duan C H and Majumdar A 2010 Anomalous ion transport in 2-nm hydrophilic nanochannels *Nature Nanotechnol.* **5** 848–52
[25] Stein D, Kruithof M and Dekker C 2004 Surface-charge-governed ion transport in nanofluidic channels *Phys. Rev. Lett.* **93** 035901
[26] Plecis A, Schoch R B and Renaud P 2005 Ionic transport phenomena in nanofluidics: experimental and theoretical study of the exclusion-enrichment effect on a chip *Nano Lett.* **5** 1147–55
[27] Karnik R, Duan C H, Castelino K, Daiguji H and Majumdar A 2007 Rectification of ionic current in a nanofluidic diode *Nano Lett.* **7** 547–51
[28] Miedema H, Vrouenraets M, Wierenga J, Meijberg W, Robillard G and Eisenberg B 2007 A biological porin engineered into a molecular, nanofluidic diode *Nano Lett.* **7** 2886–91
[29] Fan R, Huh S, Yan R, Arnold J and Yang P D 2008 Gated proton transport in aligned mesoporous silica films *Nature Mater.* **7** 303–7
[30] Gajar S A and Geis M W 1992 An ionic liquid-channel field-effect transistor *J. Electrochem. Soc.* **139** 2833–40

[31] Fan R, Yue M, Karnik R, Majumdar A and Yang P D 2005 Polarity switching and transient responses in single nanotube nanofluidic transistors *Phys. Rev. Lett.* **95** 086607

[32] Karnik R, Fan R, Yue M, Li D Y, Yang P D and Majumdar A 2005 Electrostatic control of ions and molecules in nanofluidic transistors *Nano Lett.* **5** 943–8

[33] Nam S W, Rooks M J, Kim K B and Rossnagel S M 2009 Ionic field effect transistors with sub-10 nm multiple nanopores *Nano Lett.* **9** 2044–8

[34] Joshi P, Smolyanitsky A, Petrossian L, Goryll M, Saraniti M and Thornton T J 2010 Field effect modulation of ionic conductance of cylindrical silicon-on-insulator nanopore array *J. Appl. Phys.* **107** 054701

[35] Jiang Z J and Stein D 2010 Electrofluidic gating of a chemically reactive surface *Langmuir* **26** 8161–73

[36] Veenhuis R B H, van der Wouden E J, van Nieuwkasteele J W, van den Berg A and Eijkel J C T 2009 Field-effect based attomole titrations in nanoconfinement *Lab Chip* **9** 3472–80

[37] Hughes C, Yeh L H and Qian S Z 2013 Field effect modulation of surface charge property and electroosmotic flow in a nanochannel: Stern layer effect *J. Phys. Chem.* C **117** 9322–31

[38] Donnan F G 1911 Theorie der membrangleichgewichte und membranpotentiale bei Vorhandensein von nicht Dialysierenden Elektrolyten ein Beitrag zur Physikalisch-Chemischen Physiologie *Z. Elektrochem. Angew. Phys. Chemie* **17** 572–81

[39] Donnan F G 1924 The theory of membrane equilibria *Chem. Rev.* **1** 73–90

[40] Sze S M 1981 *Physics of Semiconductor Devices* (New York: Wiley)

[41] Zangle T A, Mani A and Santiago J G 2010 Theory and experiments of concentration polarization and ion focusing at microchannel and nanochannel interfaces *Chem. Soc. Rev.* **39** 1014–35

[42] Kim S J, Song Y A and Han J 2010 Nanofluidic concentration devices for biomolecules utilizing ion concentration polarization: theory, fabrication, and applications *Chem. Soc. Rev.* **39** 912–22

[43] Plecis A, Pallandre A and Haghiri-Gosnet A M 2011 Ionic and mass transport in micro-nanofluidic devices: a matter of volumic surface charge *Lab Chip* **11** 795–804

[44] Mijatovic D, Eijkel J C T and van den Berg A 2005 Technologies for nanofluidic systems: top-down versus bottom-up—a review *Lab Chip* **5** 492–500

[45] Perry J L and Kandlikar S G 2006 Review of fabrication of nanochannels for single phase liquid flow *Microfluid. Nanofluid.* **2** 185–93

[46] Lemay S G 2010 Fluidics meets electronics: carbon nanotubes as nanopores *Chem. Int. Edn* **49** 7627–8

[47] Fan R, Karnik R, Yue M, Li D Y, Majumdar A and Yang P D 2005 DNA translocation in inorganic nanotubes *Nano Lett.* **5** 1633–7

[48] Lee C Y, Choi W, Han J H and Strano M S 2010 Coherence resonance in a single-walled carbon nanotube ion channel *Science* **329** 1320–4

[49] Wu J, Gerstandt K, Zhang H B, Liu J and Hinds B J 2012 Electrophoretically induced aqueous flow through single-walled carbon nanotube membranes *Nature Nanotechnol.* **7** 133–9

[50] Pang P, He J, Park J H, Krstic P S and Lindsay S 2011 Origin of giant ionic currents in carbon nanotube channels *ACS Nano* **5** 7277–83

[51] Schmuhl R, Keizer K, van den Berg A, ten Elshof J E and Blank D H A 2004 Controlling the transport of cations through permselective mesoporous alumina layers by manipulation of electric field and ionic strength *J. Colloid Interface Sci.* **273** 331–8

[52] Daiguji H, Hwang J, Takahashi A, Kataoka S and Endo A 2012 Ion transport in mesoporous silica SBA-16 thin films with 3D cubic structures *Langmuir* **28** 3671–7

[53] Mauritz K A and Moore R B 2004 State of understanding of Nafion *Chem. Rev.* **104** 4535–85

[54] Deml A M, Bunge A L, Reznikov M A, Kolessov A and O'Hayre R P 2012 Progress toward a solid-state ionic field effect transistor *J. Appl. Phys.* **111** 074511

[55] Goldberger J, Fan R and Yang P D 2006 Inorganic nanotubes: a novel platform for nanofluidics *Acc. Chem. Res.* **39** 239–48

[56] Cheng L J and Guo L J 2009 Ionic current rectification, breakdown, and switching in heterogeneous oxide nanofluidic devices *ACS Nano* **3** 575–84

[57] Duffy D C, McDonald J C, Schueller O J A and Whitesides G M 1998 Rapid prototyping of microfluidic systems in poly(dimethylsiloxane) *Anal. Chem.* **70** 4974–84

[58] Melosh N A, Boukai A, Diana F, Gerardot B, Badolato A, Petroff P M and Heath J R 2003 Ultrahigh-density nanowire lattices and circuits *Science* **300** 112–5

[59] Vermesh U, Choi J W, Vermesh O, Fan R, Nagarah J and Heath J R 2009 Fast nonlinear ion transport via field-induced hydrodynamic slip in sub-20-nm hydrophilic nanofluidic transistors *Nano Lett.* **9** 1315–9

[60] Cheng L J and Guo L J 2007 Rectified ion transport through concentration gradient in homogeneous silica nanochannels *Nano Lett.* **7** 3165–71

[61] Karnik R, Castelino K, Fan R, Yang P and Majumdar A 2005 Effects of biological reactions and modifications on conductance of nanofluidic channels *Nano Lett.* **5** 1638–42

[62] Wei R S, Gatterdam V, Wieneke R, Tampe R and Rant U 2012 Stochastic sensing of proteins with receptor-modified solid-state nanopores *Nature Nanotechnol.* **7** 257–63

[63] Howorka S and Siwy Z 2009 Nanopore analytics: sensing of single molecules *Chem. Soc. Rev.* **38** 2360–84

[64] Talaga D S and Li J L 2009 Single-molecule protein unfolding in solid state nanopores *J. Am. Chem. Soc.* **131** 9287–97

[65] Lee C S, Blanchard W C and Wu C T 1990 Direct control of the electroosmosis in capillary zone electrophoresis by using an external electric-field *Anal. Chem.* **62** 1550–2

[66] Hayes M A and Ewing A G 1992 Electroosmotic flow-control and monitoring with an applied radial voltage for capillary zone electrophoresis *Anal. Chem.* **64** 512–6

[67] Plecis A, Tazid J, Pallandre A, Martinhon P, Deslouis C, Chen Y and Haghiri-Gosnet A M 2010 Flow field effect transistors with polarisable interface for EOF tunable microfluidic separation devices *Lab Chip* **10** 1245–53

[68] Yeh L H, Xue S, Joo S W, Qian S and Hsu J P 2012 Field effect control of surface charge property and electroosmotic flow in nanofluidics *J. Phys. Chem.* C **116** 4209–16

[69] Oh Y J, Garcia A L, Petsev D N, Lopez G P, Brueck S R J, Ivory C F and Han S M 2009 Effect of wall–molecule interactions on electrokinetic transport of charged

molecules in nanofluidic channels during FET flow control *Lab Chip* **9** 1601–8
[70] Hayes M A 1999 Extension of external voltage control of electroosmosis to high-pH buffers *Anal. Chem.* **71** 3793–8
[71] van der Wouden E J, Hermes D C, Gardeniers J G E and van den Berg A 2006 Directional flow induced by synchronized longitudinal and zeta-potential controlling AC-electrical fields *Lab Chip* **6** 1300–5
[72] Daiguji H, Yang P D and Majumdar A 2004 Ion transport in nanofluidic channels *Nano Lett.* **4** 137–42
[73] Kim B, Heo J, Kwon H J, Cho S J, Han J, Kim S J and Lim G 2013 Tunable ionic transport for a triangular nanochannel in a polymeric nanofluidic system *ACS Nano* **7** 740–7
[74] Mafe S, Manzanares J A and Ramirez P 2010 Gating of nanopores: modeling and implementation of logic gates *J. Phys. Chem.* C **114** 21287–90
[75] Ai Y, Liu J, Zhang B K and Qian S 2010 Field effect regulation of DNA trans location through a nanopore *Anal. Chem.* **82** 8217–25
[76] Paik K H, Liu Y, Tabard-Cossa V, Waugh M J, Huber D E, Provine J, Howe R T, Dutton R W and Davis R W 2012 Control of DNA capture by nanofluidic transistors *ACS Nano* **6** 6767–75
[77] Stern M B, Geis M W and Curtin J E 1997 Nanochannel fabrication for chemical sensors *J. Vac. Sci. Technol.* B **15** 2887–91
[78] Cheng L J and Guo L J 2010 Nanofluidic diodes *Chem. Soc. Rev.* **39** 923–38
[79] Smith P L, Baukrowitz T and Yellen G 1996 The inward rectification mechanism of the HERG cardiac potassium channel *Nature* **379** 833–6
[80] Wei C, Bard A J and Feldberg S W 1997 Current rectification at quartz nanopipet electrodes *Anal. Chem.* **69** 4627–33
[81] Siwy Z, Gu Y, Spohr H A, Baur D, Wolf-Reber A, Spohr R, Apel P and Korchev Y E 2002 Rectification and voltage gating of ion currents in a nanofabricated pore *Europhys. Lett.* **60** 349–55
[82] Cervera J, Schiedt B, Neumann R, Mafe S and Ramirez P 2006 Ionic conduction, rectification, and selectivity in single conical nanopores *J. Chem. Phys.* **124** 104706
[83] Perry J M, Zhou K M, Harms Z D and Jacobson S C 2010 Ion transport in nanofluidic funnels *ACS Nano* **4** 3897–902
[84] Yan R X, Liang W J, Fan R and Yang P D 2009 Nanofluidic diodes based on nanotube heterojunctions *Nano Lett.* **9** 3820–5
[85] Vlassiouk I and Siwy Z S 2007 Nanofluidic diode *Nano Lett.* **7** 552–6
[86] Alcaraz A, Ramirez P, Garcia-Gimenez E, Lopez M L, Andrio A and Aguilella V M 2006 A pH-tunable nanofluidic diode: electrochemical rectification in a reconstituted single ion channel *J. Phys. Chem.* B **110** 21205–9
[87] Yameen B, Ali M, Neumann R, Ensinger W, Knoll W and Azzaroni O 2010 Proton-regulated rectified ionic transport through solid-state conical nanopores modified with phosphate-bearing polymer brushes *Chem. Commun.* **46** 1908–10
[88] Ali M, Ramirez P, Mafe S, Neumann R and Ensinger W 2009 A pH-tunable nanofluidic diode with a broad range of rectifying properties *ACS Nano* **3** 603–8
[89] Macrae M X, Blake S, Mayer M and Yang J 2010 Nanoscale ionic diodes with tunable and switchable rectifying behavior *J. Am. Chem. Soc.* **132** 1766–7
[90] He Y, Gillespie D, Boda D, Vlassiouk I, Eisenberg R S and Siwy Z S 2009 Tuning transport properties of nanofluidic devices with local charge inversion *J. Am. Chem. Soc.* **131** 5194–202
[91] Olthuis W, Schippers B, Eijkel J and van den Berg A 2005 Energy from streaming current and potential *Sensors Actuators* B **111** 385–9
[92] van der Heyden F H J, Bonthuis D J, Stein D, Meyer C and Dekker C 2007 Power generation by pressure-driven transport of ions in nanofluidic channels *Nano Lett.* **7** 1022–5
[93] Xie Y B, Wang X W, Xue J M, Jin K, Chen L and Wang Y G 2008 Electric energy generation in single track-etched nanopores *Appl. Phys. Lett.* **93** 163116
[94] Dlugolecki P, Nymeijer K, Metz S and Wessling M 2008 Current status of ion exchange membranes for power generation from salinity gradients *J. Membr. Sci.* **319** 214–22
[95] Kim D K, Duan C H, Chen Y F and Majumdar A 2010 Power generation from concentration gradient by reverse electrodialysis in ion-selective nanochannels *Microfluid. Nanofluid.* **9** 1215–24
[96] Min J Y, Hasselbrink E F and Kim S J 2004 On the efficiency of electrokinetic pumping of liquids through nanoscale channels *Sensors Actuators* B **98** 368–77
[97] Xuan X C and Li D Q 2006 Thermodynamic analysis of electrokinetic energy conversion *J. Power Sources* **156** 677–84
[98] Ren Y Q and Stein D 2008 Slip-enhanced electrokinetic energy conversion in nanofluidic channels *Nanotechnology* **19** 195707
[99] Davidson C and Xuan X C 2008 Electrokinetic energy conversion in slip nanochannels *J. Power Sources* **179** 297–300
[100] Guan W H and Reed M A 2012 Electric field modulation of the membrane potential in solid-state ion channels *Nano Lett.* **12** 6441–7
[101] Lakshminarayanaiah N 1984 *Equations of Membrane Biophysics* (New York: Academic)
[102] van der Heyden F H J, Stein D, Besteman K, Lemay S G and Dekker C 2006 Charge inversion at high ionic strength studied by streaming currents *Phys. Rev. Lett.* **96** 224502
[103] Zheng Z, Hansford D J and Conlisk A T 2003 Effect of multivalent ions on electroosmotic flow in micro- and nanochannels *Electrophoresis* **24** 3006–17